

# Nonlinear redshift-space distortions on the full sky

Lawrence Dam<sup>\*</sup> and Camille Bonvin<sup>†</sup>

*Département de Physique Théorique and Centre for Astroparticle Physics, Université de Genève,  
24 quai Ernest-Ansermet, CH-1211 Genève 4, Switzerland*



(Received 11 July 2023; accepted 3 October 2023; published 6 November 2023)

We derive an analytic expression for the two-point correlation function in redshift space which (i) is nonlinear (ii) is valid on the full sky, i.e. the distant-observer limit is not assumed, (iii) can account for the effect of magnification and evolution bias due to a nonuniform selection function, and (iv) respects the fact that observations are made on the past light cone, so naturally yields unequal-time correlations. Our model is based on an exact treatment of the streaming model in the wide-angle regime. Within this general regime, we find that the redshift-space correlation function is essentially determined by a geometric average of its real-space counterpart. We show that the linear expression for the galaxy overdensity, accurate to subleading order, can be recovered from our nonlinear framework. This work is particularly relevant for the modeling of odd multipoles of the correlation function at small separations and low redshifts, where wide-angle effects, selection effects, and nonlinearities are expected to be equally important.

DOI: [10.1103/PhysRevD.108.103505](https://doi.org/10.1103/PhysRevD.108.103505)

## I. INTRODUCTION

Redshift-space distortions (RSD) have been identified as a key observable to test the laws of gravity and probe the validity of the  $\Lambda$ CDM model [1]. Typically one treats RSD in the flat-sky regime, or distant-observer limit. In this regime, the redshift-space correlation function takes a simple form with a multipole structure consisting of a monopole, quadrupole, and hexadecapole [2,3]. However, this approximation is only valid over a limited range of separations and opening angles. At small separations, nonlinearities become relevant and need to be included in the modeling; whereas at large separations and opening angles, the flat-sky approximation breaks down and wide-angle effects need to be accounted for. These two types of corrections are usually treated separately: either one models the linear correlation function with wide-angle corrections, or one models the flat-sky correlation function in the nonlinear regime. In most cases, these separate approaches are enough to provide a precise description of the signal.

Besides a desire for a general model, there are two situations where both wide-angle corrections and nonlinear effects might become relevant over the same range of scales. The first concerns measurements of the correlation function at very low redshift, such as those expected from the Dark Energy Spectroscopic Instrument (DESI) [4]. In particular, the Bright Galaxy Survey sample of DESI has a very high number density of galaxies at low redshift (with median  $z \approx 0.2$ ), over  $14,000 \text{ deg}^2$  [5]. At these redshifts,

nonlinear evolution might be expected to be relevant up to relatively large separations, while wide-angle effects are expected to be important down to relatively small separations [6]. These effects are indeed governed by the ratio of pair separation  $s$  to distance  $d$ , which quickly becomes non-negligible for small  $d$ . A nonlinear model on the full sky may therefore be needed for this type of survey.

The second situation concerns the measurement of relativistic effects [7–10], where wide-angle effects and nonlinearities are both important over the same range of scales. Relativistic effects have been shown to contribute to the correlation function by generating odd multipoles (a dipole and an octupole) in the correlation of two populations of galaxies [11–13]. Both in the linear regime [12] and in the perturbative nonlinear regime, wide-angle effects are roughly of the same order of magnitude as relativistic effects. This is because relativistic effects scale as  $\mathcal{H}/k \times \text{RSD}$ , while wide-angle effects scale as  $s/d \times \text{RSD}$  [12]. These two types of effects are therefore roughly of the same order of magnitude at all scales, since  $s/d \sim \mathcal{H}/k$ .<sup>1</sup> As a consequence, if one wants, for example, to measure through the dipole the relativistic effects in the nonlinear regime, it is necessary to model at the same time wide-angle effects in this regime.

A number of works have studied various aspects of the problem. Castorina and White [14] calculated the impact of wide-angle corrections on the even multipoles, modeled

<sup>\*</sup>lawrence.dam@unige.ch

<sup>†</sup>camille.bonvin@unige.ch

<sup>1</sup>This is of course a crude comparison, since on the one hand the ratio of  $\mathcal{H}$  and  $d$  varies with redshift, and on the other hand RSD and relativistic effects are also redshift dependent. However, it shows that wide-angle effects and relativistic effects have a similar scaling and cannot be treated separately, even for large  $k$ .

using the resummed approach to Lagrangian perturbation theory (LPT) [15,16]. Their work showed that linear theory is adequate to describe wide-angle corrections for the even multipoles, except around the baryon acoustic peak where nonperturbative corrections are known to be important [17]. However, their model misses a contribution related to the (uniform) selection function. This was pointed out by Taruya *et al.* [18], who presented a model similar to that of Castorina and White, but without this deficiency (see also Refs. [19,20] for subsequent work including the gravitational redshift). A comparison with simulations showed that the contribution from the selection function is important for an accurate prediction of the dipole moment (though not for the even multipoles). Both of these works did not consider contributions from a *nonuniform* radial selection function. It is however known that in the linear regime a nonuniform selection function generates contributions from the magnification bias, which are of the same order of magnitude as wide-angle effects [21], and may even dominate the signal for some choices of populations [22].

Concerning the second situation, Beutler and di Dio [23,24] proposed a method to compute the relativistic power spectrum, including selection effects and wide-angle effects in perturbation theory. They derived an expression for the dipole, including contributions up to third order in perturbation theory, which agrees well with numerical simulations up to  $k_{\max} \simeq 0.4h^{-1}$  Mpc. More recently, Noorikuhani and Scoccimarro [25] calculated the impact of relativistic effects and wide-angle corrections on the galaxy power spectrum and bispectrum. Their approach was to model these Fourier statistics in the usual way—i.e. work in the distant-observer limit and use one-loop perturbation theory—but supplement with the leading-order relativistic and wide-angle contributions. This hybrid approach was justified on the basis that the nonlinearities were found not to mix significantly with the relativistic and wide-angle effects.

This paper begins a study of these two situations from an altogether different approach. Here we will largely focus on the first situation, exhibiting a novel approach to the streaming model [26,27], a nonlinear model of the RSD correlation function; a forthcoming work will be dedicated to a complete model for the second situation. We will thus show how the streaming model can be exactly extended to the wide-angle regime, taking advantage of the simple geometry of the problem in configuration space. This model is similar in some respects to that of Taruya *et al.* [18] but differs importantly in others. In particular, here we allow for the more realistic case of a nonuniform selection function, which leads to further distortions through the magnification and evolution bias. In addition, here we derive in full generality the relation between the matter density field in redshift space and in real space, independent of the details of how such fields might evolve or might

be biased in relation to the galaxy field. (The dynamics and galaxy bias can be specified, for example, using the “convolution LPT” prescription [28–30], as has proven a powerful method.)

Based on a more general treatment of the redshift mapping and number conservation, we will further show that the streaming model can also accommodate selection, galaxy evolution, and relativistic effects—indeed, almost all subleading effects at  $\mathcal{O}(\mathcal{H}/k)$ . These effects, as mentioned, are of the same order as the wide-angle effects so in principle should also be taken into account. With the streaming model, these effects are logically separated and enter in resummed form, thereby offering a compact way of capturing the large number of terms that contribute to the overdensity at subleading order (i.e. when expressed through a perturbative expansion). Additionally, its modular form lends itself well to the problem of modeling at the same time the three different kinds of sources of nonlinearity that need to be considered in a realistic model—namely, dynamics, galaxy bias, and the redshift mapping (wide-angle effects in our model are exact to all orders in  $s/d$ ).

The outline of this paper is as follows. In Sec. II we extend the nonlinear approach to RSD [26] to the wide-angle regime, deriving a nonperturbative expression for the wide-angle correlation function in redshift space. In Sec. III we extend the derivation to construct a more realistic model of the correlation function which takes into account selection effects, as well as the fact that observations are made on the light cone. We then perform a perturbative expansion of our model in Sec. IV and show that well-known results from linear theory are recovered, including of many relativistic effects. In Sec. V we present the full-sky generalization of the Gaussian streaming model, and show that it is consistent with the expected form in the distant-observer limit. In Sec. VI we calculate the linear theory multipoles including wide-angle contributions, and show that they are consistent with expressions found in the literature. Our conclusions follow in Sec. VII. Several appendixes describe the details of our calculations.

## II. NONLINEAR MODELING IN THE WIDE-ANGLE REGIME

This section is principally devoted to a study of the relation between a galaxy at its true (comoving) position  $\mathbf{x}$  and its observed (comoving) position  $\mathbf{s}$ ,

$$\mathbf{s}(\mathbf{x}) = \mathbf{x} + \hat{\mathbf{x}} \cdot \mathbf{u}(\mathbf{x}) \hat{\mathbf{x}}, \quad (1)$$

as concerns the correlation function in redshift space. Here  $\mathbf{u} = \mathcal{H}^{-1} \mathbf{v}$  (which has units of length),  $\mathbf{v}$  is the peculiar velocity, and  $\mathcal{H}$  is the conformal Hubble parameter. This mapping of course leads to the well-known Kaiser effect, typically modeled in the distant-observer limit in which one assumes that distant objects have identical line of sight  $\hat{\mathbf{x}}$ .

This approximation is valid for small opening angles between any two lines of sight in a galaxy sample.

Here we present an exact treatment of the general case in which lines of sight  $\hat{\mathbf{x}}$  are allowed to vary across the full sky without restriction to small angles. To highlight the key trick in this paper and make clear the geometric interpretation, we will first present the calculation of the full-sky correlation function without any complicating factors such as selection effects. We will also focus on equal-time correlations and suppress the time dependence in the number density, velocity, etc.; we will restore it in Sec. III when we come to consider unequal-time correlations on the light cone and related projection effects.

The basis of our approach is the number of conservation of objects in real and redshift space:

$$n_s(\mathbf{s})d^3\mathbf{s} = n(\mathbf{x})d^3\mathbf{x}, \quad (2)$$

where  $n(\mathbf{x})$  and  $n_s(\mathbf{s})$  are the comoving number densities in real and redshift space, respectively. In integral form, we have equivalently

$$n_s(\mathbf{s}) = \int d^3\mathbf{x} n(\mathbf{x}) \delta_{\text{D}}(\mathbf{s} - \mathbf{s}(\mathbf{x})). \quad (3)$$

This expression in fact holds for general mappings  $\mathbf{s}(\mathbf{x})$ —not just for Eq. (1)—including those that also contain transverse displacements. It also holds in the regime of multiple streams, i.e. when more than one point in real space formally maps to a single point in redshift space [when  $\mathbf{s}(\mathbf{x})$  has singular Jacobian].

Now, since we work on the full sky and since the mapping only affects the radial positions, it is natural to switch to a spherical coordinate system. Thus let  $\chi = |\mathbf{s}|$  be the (observed) radial distance in redshift space and  $\chi' = |\mathbf{x}|$  the radial distance in real space. Writing Eq. (3) in spherical coordinates, separating the Dirac delta function into a radial piece and an angular piece, and inserting  $n_s(\mathbf{s}) = \bar{n}_s[1 + \delta_s(\mathbf{s})]$  and  $n(\mathbf{x}) = \bar{n}[1 + \delta(\mathbf{x})]$  (here  $\bar{n}_s$  and  $\bar{n}$  denote the mean number densities in redshift and real space, respectively), we have

$$1 + \delta_s(\mathbf{s}) = \int_0^\infty d\chi' \chi'^2 \int d^2\hat{\mathbf{x}} [1 + \delta(\mathbf{x})] \times \frac{1}{\chi^2} \delta_{\text{D}}(\chi - \chi' - \hat{\mathbf{x}} \cdot \mathbf{u}(\mathbf{x})) \delta_{\text{D}}(\hat{\mathbf{n}} - \hat{\mathbf{x}}), \quad (4)$$

where  $\hat{\mathbf{n}} = \mathbf{s}/|\mathbf{s}|$  is the line of sight, and we have furthermore used that, in the absence of selection or evolution effects, the mean densities in real and redshift space are equal,  $\bar{n} = \bar{n}_s$ ; see Appendix A for justification. Parametrizing the positions as  $\mathbf{s} = \chi\hat{\mathbf{n}}$  and  $\mathbf{x} = \chi'\hat{\mathbf{x}}$ , and doing the trivial angular integral, we get

$$1 + \delta_s(\chi\hat{\mathbf{n}}) = \frac{1}{\chi^2} \int_0^\infty d\chi' \chi'^2 [1 + \delta(\chi'\hat{\mathbf{n}})] \times \delta_{\text{D}}(\chi - \chi' - \hat{\mathbf{n}} \cdot \mathbf{u}(\chi'\hat{\mathbf{n}})) \quad (5)$$

$$= \frac{1}{\chi^2} \int_0^\infty d\chi' \chi'^2 [1 + \delta(\chi'\hat{\mathbf{n}})] \times \int_{-\infty}^\infty \frac{dk}{2\pi} e^{-ik(\chi-\chi')} e^{iku_{\parallel}(\chi'\hat{\mathbf{n}})}, \quad (6)$$

where in the second line the Dirac delta function is given as its Fourier representation, writing  $u_{\parallel} = \hat{\mathbf{n}} \cdot \mathbf{u}$  for the radial component of the velocity. As we will show in Sec. IV, this equation recovers at linear order the familiar Kaiser term, including the subdominant inverse-distance term. With Eq. (6) it is straightforward to obtain the correlation function  $\xi_s = \langle \delta_s(\mathbf{s}_1) \delta_s(\mathbf{s}_2) \rangle$ :

$$1 + \xi_s(\chi_1, \chi_2, \hat{\mathbf{n}}_1 \cdot \hat{\mathbf{n}}_2) = \frac{1}{\chi_1^2 \chi_2^2} \int d\chi'_1 \chi'^2_1 \int d\chi'_2 \chi'^2_2 \times \int \frac{d^2\boldsymbol{\kappa}}{(2\pi)^2} e^{-i\boldsymbol{\kappa} \cdot (\chi - \chi')} \langle [1 + \delta(\chi'_1 \hat{\mathbf{n}}_1)] \times [1 + \delta(\chi'_2 \hat{\mathbf{n}}_2)] e^{i\boldsymbol{\kappa} \cdot \mathbf{w}} \rangle \quad (7)$$

$$= \frac{1}{\chi_1^2 \chi_2^2} \int d\chi'_1 \chi'^2_1 \int d\chi'_2 \chi'^2_2 [1 + \xi(r)] \times \int \frac{d^2\boldsymbol{\kappa}}{(2\pi)^2} e^{-i\boldsymbol{\kappa} \cdot (\chi - \chi')} \langle e^{i\boldsymbol{\kappa} \cdot \mathbf{w}} \rangle_{\delta}, \quad (8)$$

where  $r = (\chi_1^2 + \chi_2^2 - 2\chi_1\chi_2 \cos \vartheta)^{1/2}$  is the separation between the two galaxies in real space,  $\cos \vartheta = \hat{\mathbf{n}}_1 \cdot \hat{\mathbf{n}}_2$  is the cosine of the opening angle, and we have defined the following two-component vectors:  $\boldsymbol{\kappa} = (k_1, k_2)$ ,  $\boldsymbol{\chi} = (\chi_1, \chi_2)$ ,  $\boldsymbol{\chi}' = (\chi'_1, \chi'_2)$ , and  $\mathbf{w} \equiv (u_{\parallel}(\mathbf{x}_1), u_{\parallel}(\mathbf{x}_2)) = (\hat{\mathbf{n}}_1 \cdot \mathbf{u}(\chi'_1 \hat{\mathbf{n}}_1), \hat{\mathbf{n}}_2 \cdot \mathbf{u}(\chi'_2 \hat{\mathbf{n}}_2))$ . Furthermore, in the second line we have identified the moment generator  $\langle e^{i\boldsymbol{\kappa} \cdot \mathbf{w}} \rangle_{\delta}$ , where in this work a subscript  $\delta$  denotes the density-weighted ensemble average

$$\langle O \rangle_{\delta} \equiv \langle [1 + \delta(\mathbf{x}_1)][1 + \delta(\mathbf{x}_2)] O \rangle / \langle [1 + \delta(\mathbf{x}_1)][1 + \delta(\mathbf{x}_2)] \rangle. \quad (9)$$

There is a more intuitive way of expressing Eq. (8). Recognizing that the  $\boldsymbol{\kappa}$  integral in Eq. (8) (the inverse Fourier transform of the generating function) defines the joint probability distribution of radial displacements,

$$p(\boldsymbol{\chi} - \boldsymbol{\chi}'; \boldsymbol{\chi}' | \hat{\mathbf{n}}_1 \cdot \hat{\mathbf{n}}_2) \equiv \int \frac{d^2\boldsymbol{\kappa}}{(2\pi)^2} e^{-i\boldsymbol{\kappa} \cdot (\boldsymbol{\chi} - \boldsymbol{\chi}')} Z(\mathbf{J} = \boldsymbol{\kappa}; \mathbf{r}(\boldsymbol{\chi}'), \hat{\mathbf{n}}_1 \cdot \hat{\mathbf{n}}_2), \quad (10)$$

$$Z(\mathbf{J}; \mathbf{r}, \hat{\mathbf{n}}_1 \cdot \hat{\mathbf{n}}_2) \equiv \langle e^{i\mathbf{J} \cdot \mathbf{w}} \rangle_{\delta},$$

we can write

$$\begin{aligned}
& 1 + \xi_s(\chi_1, \chi_2, \hat{\mathbf{n}}_1 \cdot \hat{\mathbf{n}}_2) \\
&= \frac{1}{\chi_1^2 \chi_2^2} \int_0^\infty d\chi'_1 \chi'^2_1 \int_0^\infty d\chi'_2 \chi'^2_2 [1 + \xi(r)] \\
&\quad \times p(\chi - \chi'; \chi' | \hat{\mathbf{n}}_1 \cdot \hat{\mathbf{n}}_2). \tag{11}
\end{aligned}$$

This formula is the full-sky generalization of the (distant-observer) streaming model [26], which is given by a single line-of-sight integral.

The probability distribution (10) is scale dependent: it depends not only on  $\chi - \chi'$  but also on  $\chi'$  itself through the moments of  $\mathbf{w}$  (by way of  $Z$ ).<sup>2</sup> The existence of coherent flows is the origin of this scale dependence, without which  $p$  is a proper probability distribution. This dependence on  $\chi'$  has the effect that as we integrate over  $\chi'_1$  and  $\chi'_2$  we pass through a two-parameter family of probability distributions, each with different mean, covariance, etc.—there is not a single fixed distribution. There is also a dependence of  $p$  on the opening angle  $\hat{\mathbf{n}}_1 \cdot \hat{\mathbf{n}}_2$  but, unlike the dependence on  $\chi'$ , is known *a priori* (as indicated by the conditional).

A useful if heuristic way to view Eq. (11) is as the expectation of  $1 + \xi(r)$  when averaged over all real-space triangles that can be formed from an opening angle  $\hat{\mathbf{n}}_1 \cdot \hat{\mathbf{n}}_2$ , e.g. by varying the adjacent side lengths  $\chi'_1$  and  $\chi'_2$ . Schematically,

$$\xi_s = \langle \xi \rangle_\Delta, \tag{12}$$

for  $\langle \cdot \rangle_\Delta$  some average over triangles. More precisely, we have a probability space of real-space triangles, parametrized relative to the fixed redshift-space triangle by  $\chi_1 - \chi'_1$  and  $\chi_2 - \chi'_2$  (see Fig. 1). These radial displacements are correlated since they are the result of Doppler shifts produced by the radial velocities  $u_{\parallel}(\chi'_1 \hat{\mathbf{n}}_1)$  and  $u_{\parallel}(\chi'_2 \hat{\mathbf{n}}_2)$ , which are themselves correlated. Since velocity correlations depend on the separation  $\mathbf{r} = \mathbf{x}_1 - \mathbf{x}_2 = \chi'_1 \hat{\mathbf{n}}_1 - \chi'_2 \hat{\mathbf{n}}_2$ , not all triangles in Eq. (11) contribute with the same probability. In particular, triangles in real space that are far from the redshift-space configuration will contribute negligibly, since no large-scale correlated flow is likely to arise that can map these configurations into each other; conversely, configurations that are close to each other will contribute significantly to the integral. How close will depend on the characteristic separation along each line of sight as determined by the means  $\langle u_{\parallel}(\mathbf{x}_1) \rangle_\delta$  and  $\langle u_{\parallel}(\mathbf{x}_2) \rangle_\delta$ .

We emphasize that no dynamical assumptions have been made in obtaining Eq. (11); it is an exact result based on the formal relation (3) between the observed and underlying

<sup>2</sup>More precisely, these velocity moments generally depend on the separation  $r$  and the projections  $\hat{\mathbf{r}} \cdot \hat{\mathbf{n}}_1$  and  $\hat{\mathbf{r}} \cdot \hat{\mathbf{n}}_2$ , which are geometrically related to  $\chi'_1$ ,  $\chi'_2$ , and  $\hat{\mathbf{n}}_1 \cdot \hat{\mathbf{n}}_2$ .

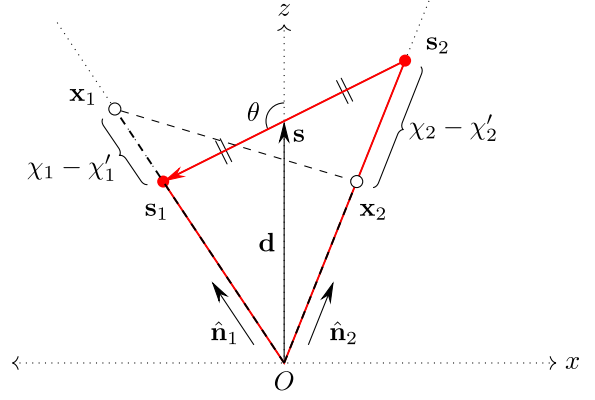


FIG. 1. Parametrization of a typical triangle configuration in the wide-angle regime. The redshift-space configuration (indicated in red) is the triangle formed by the observer  $O$  together with the galaxies at observed positions  $\mathbf{s}_1$  and  $\mathbf{s}_2$ . An example of a real-space configuration (dashed black) that could map onto the redshift-space triangle is indicated by the triangle formed by  $\mathbf{x}_1$ ,  $\mathbf{x}_2$ , and  $O$ . Note that candidates for the true positions,  $\mathbf{x}_1$  and  $\mathbf{x}_2$ , can lie anywhere on the respective lines of sight, and the probability of a given candidate triangle mapping onto the observed triangle is determined by the joint distribution of the separations  $\chi_1 - \chi'_1$  and  $\chi_2 - \chi'_2$ . Here  $\hat{\mathbf{n}}_1$  and  $\hat{\mathbf{n}}_2$  are fixed, and we have aligned the  $z$  axis to bisect the separation  $\mathbf{s} = \mathbf{s}_1 - \mathbf{s}_2$  at the mid-point  $\mathbf{d} = (\mathbf{s}_1 + \mathbf{s}_2)/2$ . Without loss of generality, the galaxy pair lives in the  $xz$  plane.

density fields.<sup>3</sup> Furthermore, we have made no attempt to account for the galaxy bias, since including it in this framework is straightforward [16,29,31]—e.g. by replacing  $1 + \delta$  with  $1 + b\delta$  (in linear theory), or, more generally, some functional of  $\delta$ . Irrespective of tracer (galaxies, halos, dark matter particles, etc.), the relation between the observed and underlying fields remains the same.

Finally, since the line-of-sight integrals in Eq. (11) are over nonoscillatory real functions, evaluating them numerically is in principle straightforward once the real-space correlation function and probability distribution are specified. (In Sec. V we explicitly show the form of these integrals in the case of the Gaussian streaming model.)

### III. A MODEL INCLUDING LIGHT CONE, SELECTION, AND EVOLUTION EFFECTS

Going beyond the distant-observer limit, wide-angle effects are among a number of effects that need to be considered all at once. We first give a physical explanation of these additional effects in Secs. III A and III B, and in Sec. III C we derive the full model including all effects.

<sup>3</sup>As with other nonlinear treatments of RSD (e.g. Ref. [26]), our model is “exact” only to the extent that the redshift mapping (1) is exact. But this mapping cannot be said to be exact as it is based on a linear approximation of the full relation between  $\mathbf{s}$  and  $\mathbf{x}$  (even if the perturbations are themselves fully nonlinear); see Sec. III A.

### A. Extending the redshift mapping to the light cone

Observations are made on the past light cone but this is not reflected in the mapping (1) nor the correlation function (11) derived from it. In particular, the mapping (1) does not take into account the fact that perturbations to the redshift also induce a displacement in the lookback time, thus changing the apparent position on the light cone. We can see this by reconsidering the problem of mapping galaxies in a redshift survey.<sup>4</sup>

The basic task is to assign Cartesian (comoving) coordinates  $\mathbf{s}$  using redshifts and angular positions. For a galaxy with measured redshift  $z$  observed in the direction  $\hat{\mathbf{x}}$ , we assign to it the coordinates  $\mathbf{s} = \chi(z)\hat{\mathbf{x}}$ , where the conversion from redshift to comoving radial distance is given by  $\chi(z) = \int_0^z dz'/H(z')$ . This is the observed position. (Here we assume perfect knowledge of the underlying background cosmology, and no angular deflections so that  $\hat{\mathbf{x}} = \hat{\mathbf{n}}$ .) The (unknown) true position is  $\mathbf{x} = \chi'\hat{\mathbf{x}}$ , where  $\chi' \equiv \chi(\bar{z})$ ,  $\bar{z} = z - \delta z$  is the background redshift and  $\delta z$  the redshift perturbation. This is the position that would be inferred had the redshift not suffered a Doppler shift. The mapping (1) is obtained by linearizing  $\mathbf{s} = \chi(\bar{z} + \delta z)\hat{\mathbf{x}}$  about the true position  $\mathbf{x} = \chi(\bar{z})\hat{\mathbf{x}}$ :

$$\mathbf{s} \simeq \chi(\bar{z})\hat{\mathbf{x}} + \delta z \left. \frac{d\chi}{dz} \right|_{z=\bar{z}} \hat{\mathbf{x}} = \mathbf{x} + \hat{\mathbf{x}} \cdot \mathbf{u}(\tau', \mathbf{x})\hat{\mathbf{x}}, \quad (13)$$

where in the second equality we have used that  $\delta z = (1 + \bar{z})\mathbf{v} \cdot \hat{\mathbf{x}}$ , obtained from the relation  $1 + z = (1 + \bar{z})(1 + \mathbf{v} \cdot \hat{\mathbf{x}})$  for the Doppler shift.

But redshift is not only an indicator of distance; it is also an indicator of time, with galaxies at larger redshifts associated with larger lookback times; see Fig. 2. So in addition to assigning spatial coordinates, we also assign a time coordinate  $\tau$  to each galaxy [12]. More precisely, following a galaxy photon along the line of sight  $\hat{\mathbf{x}}$  back to the observed redshift  $z$ , we assign

$$\tau = \tau_0 - \chi(z), \quad (14)$$

the time at which the photon was apparently emitted. Here  $\tau_0$  is the present conformal time. Likewise, we have for the real time  $\tau' = \tau_0 - \chi'$ . The relation between  $\tau'$  and  $\tau$  is then given by linearizing  $\tau(z) = \tau(\bar{z} + \delta z)$  about  $\tau(\bar{z}) \equiv \tau'$ . At linear order we have  $\tau \simeq \tau' - u_{\parallel}(\tau', \mathbf{x})$ , which together with Eq. (1) constitutes a map  $(\tau', \mathbf{x}) \mapsto (\tau, \mathbf{s})$  on the light cone. Note that  $\tau'$  is in fact degenerate with  $\mathbf{x}$  since  $\tau' = \tau_0 - \chi'$  and  $\chi' = |\mathbf{x}|$ , and that the displacement on the light cone is null:  $-(\tau - \tau')^2 + (\chi - \chi')^2 = 0$ .

In the rest of this section we will work with this spacetime mapping. As we will see in Sec. III C, any

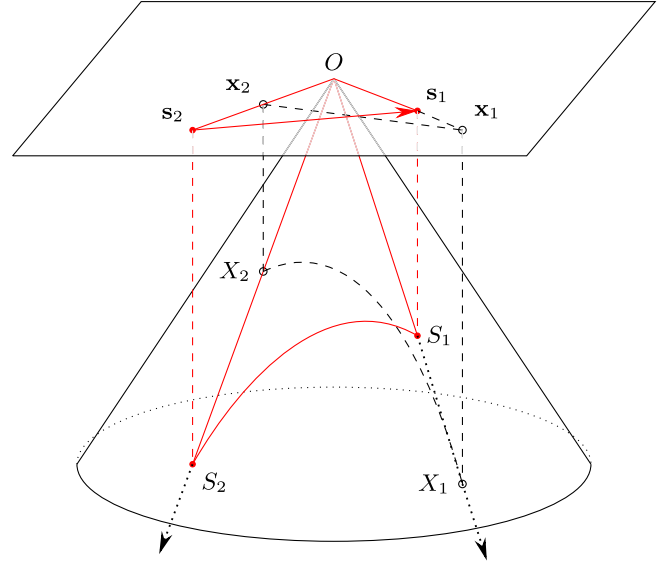


FIG. 2. Configurations on the past light cone and their spatial projections. The observed configuration is shown in red, while a potential true configuration is shown in black. Here  $S_i = (\tau_0 - \chi_i, \mathbf{s}_i)$  is the assigned spacetime position, while  $X_i = (\tau_0 - \chi'_i, \mathbf{x}_i)$  is the real spacetime position, i.e. the position that would be observed absent all distortions to the redshift. The two-point correlation between  $S_1$  and  $S_2$  is determined by all two-point correlations between possible  $X_1$  and  $X_2$  falling on the lines of sight (dotted lines).

evolution in the number density between the surface of constant  $\tau$  (constant observed redshift  $z$ ) and the surface of constant  $\tau'$  (constant background redshift  $\bar{z}$ ) gives rise to an apparent density fluctuation. These distortions are among some of the many contributions to the full expression for the overdensity derived using relativistic perturbation theory. While subdominant to the Kaiser effect, these projection effects are of the same order as wide-angle effects so in principle should also be included.

### B. Selection effects

In addition to projection effects related to the light cone, we also need to take into account the selection effects. These give rise to fluctuations of order  $\mathcal{H}/k$  which, although subdominant to the usual RSD, are of the same size as the wide-angle corrections so cannot generally be ignored.

#### 1. Flux limit

Since surveys only observe above a certain flux limit  $F_*$ , not all sources in the sky will be bright enough to be detected. This is seen in the observed mean number density, or selection function  $\bar{n}_s(\chi, F > F_*)$ , which tends to fall off with distance  $\chi$ . In general, we do *not* have  $\bar{n}_s = \bar{n}$  (where  $\bar{n}$  is the selection function in real space), since some sources that would otherwise not be detectable in real space can be seen in redshift space due to magnification effects (and vice versa). The difference between the two effectively

<sup>4</sup>See Ref. [10] for a discussion of the general problem in terms of photon geodesics.

generates an additional density fluctuation. Note that the selection function provides a complete description of the selection effect in the nonlinear regime; however, in linear theory the relevant quantity is the linear response of the selection function to a change in the flux limit, i.e. the slope of  $\bar{n}_s$  with respect to the threshold:

$$s_* \equiv \frac{\partial \log \bar{n}_s}{\partial m_*} = -\frac{2}{5} \frac{\partial \ln \bar{n}_s}{\partial \ln F_*} = -\frac{2}{5} \frac{\partial \ln \bar{n}_s}{\partial \ln L_*}, \quad (15)$$

where  $m_* = -2.5 \log F_* + \text{const}$  is the magnitude limit and  $F_*$  ( $L_*$ ) is the flux (luminosity) limit of the survey. This parameter (not to be confused with the redshift coordinates) is known as the ‘‘magnification bias’’ and is survey and population dependent.

## 2. Galaxy evolution

Galaxies can merge with each other or be created altogether. This was not reflected in the model (11) which assumed a constant number of galaxies ( $\bar{n}_s = \bar{n} = \text{const}$ ). Since the time evolution of the mean comoving number density  $\bar{n}(\tau)$  depends upon the uncertain details of galaxy formation and evolution, it is conventionally parametrized by the ‘‘evolution bias’’

$$f_{\text{evol}} \equiv \frac{\partial \ln \bar{n}}{\partial \ln a}; \quad \bar{n}(\tau) = F_{\text{evol}}(\tau) \bar{n}(\tau_0),$$

$$F_{\text{evol}}(\tau) \equiv \exp\left(-\int_{a(\tau)}^1 \frac{da'}{a'} f_{\text{evol}}(a')\right). \quad (16)$$

With no evolution,  $f_{\text{evol}} = 0$  and  $F_{\text{evol}} = 1$  for all time. In general,  $f_{\text{evol}}$  is tracer dependent and a function of the flux cut. Note that the effect of galaxy evolution on the apparent number density may be considered an example of a projection effect, in that the lookback time (14) of a galaxy viewed in real space is different to the lookback time of the same galaxy but viewed in redshift space.

## C. Derivation of the general model

We now construct a model of the redshift-space correlation function valid on the full sky and in the nonlinear regime, building into it the lookback time (14), as well as the flux cut and galaxy evolution. The calculation is essentially the same as before once we have set up the problem and introduced some definitions. Readers who are not interested in these details may skip ahead to Eq. (31) and follow the discussion from there.

To include a flux cut in the model we now need to consider the luminosity of each galaxy. We define the redshift-space distribution function  $\Phi_s(\tau, \mathbf{s}, F_s)$ , i.e. the redshift-space comoving number density of galaxies in the flux bin  $(F_s, F_s + dF_s)$ . Similarly, let  $\Phi(\tau, \mathbf{x}, F)$  be the true distribution function, i.e. the real-space comoving number

density of galaxies in the (nonredshifted) flux bin  $(F, F + dF)$ .

Since the mapping  $(\tau', \mathbf{x}) \mapsto (\tau(\mathbf{x}), \mathbf{s}(\mathbf{x}))$ , where  $\tau(\mathbf{x})$  is the lookback time (14) and  $\mathbf{s}(\mathbf{x})$  is given by Eq. (1), is nothing more than a reassignment of each galaxy’s coordinates, the number of galaxies per flux bin is conserved:

$$\Phi_s(\tau, \mathbf{s}, F_s) d^3 \mathbf{s} dF_s = \Phi(\tau', \mathbf{x}, F) d^3 \mathbf{x} dF$$

$$= \Phi(\tau', \mathbf{x}, L) d^3 \mathbf{x} dL, \quad (17)$$

where  $\tau' = \tau_0 - \chi'$  and, in a slight abuse of notation,  $\Phi(\tau', \mathbf{x}, F) = \Phi(\tau', \mathbf{x}, L) dL/dF$ . Here  $\tau = \tau_0 - \chi$  and  $\tau' = \tau_0 - \chi'$ , and we recall that these are related by  $\tau = \tau' - u_{\parallel}$ . Equation (17) simply reflects the fact that all galaxies that are observed in  $d^3 \mathbf{s}$  with flux between  $F_s$  and  $F_s + dF_s$  physically lie in  $d^3 \mathbf{x}$  with intrinsic luminosity between  $L$  and  $L + dL$ . Among all the galaxies in the volume element  $d^3 \mathbf{s}$  or  $d^3 \mathbf{x}$ , we select only those that meet or exceed the flux threshold  $F_*$ :

$$\Theta(F_s - F_*) \Phi_s(\tau, \mathbf{s}, F_s) d^3 \mathbf{s} dF_s$$

$$= \Theta(L - L_*(\mathbf{x})) \Phi(\tau', \mathbf{x}, L) d^3 \mathbf{x} dL. \quad (18)$$

Here  $\Theta$  is the Heaviside step function which enforces the threshold and  $L_*(\mathbf{x}) = 4\pi d_L^2(\mathbf{x}) F_*$  is the luminosity threshold for an object at luminosity distance  $d_L(\mathbf{x})$ . Note that on both sides of Eq. (18) we are imposing the same selection criterion so that the same galaxies are being selected in both real and redshift space. Since the luminosity distance  $d_L$  is affected by inhomogeneities and depends therefore on direction, a fixed flux threshold  $F_*$  in all directions corresponds to different luminosity thresholds  $L_*(\mathbf{x})$  in different directions.

Integrating both sides of Eq. (18) yields the differential relation between number densities [cf. Eq. (2)]

$$n_s(\tau, \mathbf{s}; F > F_*) d^3 \mathbf{s} = n(\tau', \mathbf{x}; L > L_*(\mathbf{x})) d^3 \mathbf{x}, \quad (19)$$

where

$$n_s(\tau, \mathbf{s}; F > F_*) \equiv \int_{F_*}^{\infty} dF_s \Phi_s(\tau, \mathbf{s}, F_s),$$

$$n(\tau', \mathbf{x}; L > L_*(\mathbf{x})) \equiv \int_{L_*(\mathbf{x})}^{\infty} dL \Phi(\tau', \mathbf{x}, L). \quad (20)$$

Separating the number densities into a mean contribution and an overdensity, assuming a universal luminosity function, we obtain

$$[1 + \delta_s(\tau, \mathbf{s})] d^3 \mathbf{s} = \frac{\bar{n}(\tau', L > L_*(\mathbf{x}))}{\bar{n}_s(\tau, F > F_*)} [1 + \delta(\tau', \mathbf{x})] d^3 \mathbf{x}. \quad (21)$$

The denominator on the right-hand side can be rewritten as

$$\bar{n}_s(\tau, F > F_*) = \bar{n}(\tau, L > \bar{L}_*(\chi)), \quad (22)$$

since the mean number of galaxies at  $\tau$  with flux above  $F_*$  corresponds to the galaxies that have mean intrinsic luminosity above  $\bar{L}_*(\chi)$ . The fraction in Eq. (21) can then be split as

$$\frac{\bar{n}(\tau', L > L_*(\mathbf{x}))}{\bar{n}(\tau, L > \bar{L}_*(\chi))} = \frac{\bar{n}(\tau', L > L_*(\mathbf{x})) \bar{n}(\tau', L > \bar{L}_*(\chi'))}{\bar{n}(\tau', L > \bar{L}_*(\chi')) \bar{n}(\tau, L > \bar{L}_*(\chi'))} \times \frac{\bar{n}(\tau, L > \bar{L}_*(\chi'))}{\bar{n}(\tau, L > \bar{L}_*(\chi))}, \quad (23)$$

which gives rise to three contributions. First  $\delta_*$ , defined as

$$1 + \delta_*(\tau', \mathbf{x}) = \frac{\bar{n}(\tau', L > L_*(\mathbf{x}))}{\bar{n}(\tau', L > \bar{L}_*(\chi'))}, \quad (24)$$

represents the fractional number density of galaxies at  $\mathbf{x}$  with luminosity comprised between  $\bar{L}_*(\chi')$  and  $L_*(\mathbf{x}) = \bar{L}_*(\chi') + \delta L_*(\chi', \hat{\mathbf{n}})$ , where the perturbation to the luminosity threshold  $\delta L_*$  is directly related to the perturbation to the luminosity distance by

$$\delta L_*(\chi', \hat{\mathbf{n}}) = 4\pi F_* [d_L^2(\chi', \hat{\mathbf{n}}) - \bar{d}_L^2(\chi')], \quad (25)$$

and is affected by the Doppler effect (among other things). Here  $\bar{L}_*(\chi') = 4\pi \bar{d}_L^2(\chi') F_*$  is the threshold that would be adopted in the absence of perturbations to the luminosity distance.

Second  $\delta_{\text{evol}}$ , defined as

$$1 + \delta_{\text{evol}}(\tau', \mathbf{x}) = \frac{\bar{n}(\tau', L > \bar{L}_*(\chi'))}{\bar{n}(\tau, L > \bar{L}_*(\chi'))}, \quad (26)$$

encodes the evolution of the comoving number density of galaxies, above a *fixed* luminosity threshold  $\bar{L}_*(\chi')$ , between the hypersurface of constant  $\tau$  (corresponding to constant observed redshift  $z$ ) and the hypersurface of constant  $\tau'$  (corresponding to constant background redshift  $\bar{z}$ ). Using Eq. (16), applied at  $\tau$  and  $\tau'$  for the same luminosity threshold  $\bar{L}_*(\chi')$ , we obtain

$$1 + \delta_{\text{evol}}(\tau', \mathbf{x}) = \frac{F_{\text{evol}}(\tau')}{F_{\text{evol}}(\tau)}. \quad (27)$$

Finally  $\delta_L$ , defined as

$$1 + \delta_L(\tau', \mathbf{x}) = \frac{\bar{n}(\tau, L > \bar{L}_*(\chi'))}{\bar{n}(\tau, L > \bar{L}_*(\chi))}, \quad (28)$$

describes the fractional number of galaxies with luminosity between  $\bar{L}_*(\chi')$  and  $\bar{L}_*(\chi)$ . (Here  $\delta_L$  is not to be confused

with the linear matter field.) This term accounts for the fact that, since we select galaxies above a fixed flux threshold  $F_*$ , we do not select the same population of galaxies at each distance. Galaxies that are further away are selected with a higher luminosity than galaxies that are closer. Because of this, even if the luminosity function would be constant in time for all values of  $L$ , there is an evolution in the mean number density.

With this, Eq. (21) becomes

$$[1 + \delta_s(\tau, \mathbf{s})] d^3 \mathbf{s} = [1 + \delta_{\text{tot}}(\tau', \mathbf{x})] d^3 \mathbf{x}, \quad (29)$$

where

$$1 + \delta_{\text{tot}}(\tau', \mathbf{x}) \equiv [1 + \delta_{\text{evol}}(\tau', \mathbf{x})][1 + \delta_L(\tau', \mathbf{x})][1 + \delta_*(\tau', \mathbf{x})] \times [1 + \delta(\tau', \mathbf{x})]. \quad (30)$$

Without selection and evolution effects, clearly  $\delta_{\text{tot}} = \delta$ .

An explicit expression for  $\delta_s$  can now be obtained by a similar calculation to the one presented in Sec. II. Thus, passing from differential to integral form (3), changing to spherical coordinates, etc., we have

$$1 + \delta_s(\tau, \chi \hat{\mathbf{n}}) = \frac{1}{\chi^2} \int_0^\infty d\chi' \chi'^2 [1 + \delta_{\text{tot}}(\tau_0 - \chi', \chi' \hat{\mathbf{n}})] \times \int \frac{d\mathbf{k}}{2\pi} e^{-ik(\chi - \chi')} \exp[ik u_{\parallel}(\tau_0 - \chi', \chi' \hat{\mathbf{n}})]. \quad (31)$$

The difference between this expression and our earlier one, Eq. (6), is that  $\delta$  there is replaced with  $\delta_{\text{tot}}$  here, and secondly the line-of-sight integral is now performed on the past light cone.

Finally, since Eq. (31) is of the same form as Eq. (6), the calculation proceeds as before and we can write down at once the correlation function [cf. Eq. (11)]:

$$1 + \xi_s(\chi_1, \chi_2, \hat{\mathbf{n}}_1 \cdot \hat{\mathbf{n}}_2) = \frac{1}{\chi_1^2 \chi_2^2} \int_0^\infty d\chi'_1 \chi'^2_1 \int_0^\infty d\chi'_2 \chi'^2_2 [1 + \xi_{\text{tot}}(\chi'_1, \chi'_2, \hat{\mathbf{n}}_1 \cdot \hat{\mathbf{n}}_2)] \times p_{\text{tot}}(\chi - \chi' | \hat{\mathbf{n}}_1 \cdot \hat{\mathbf{n}}_2) \text{ with} \\ 1 + \xi_{\text{tot}}(\chi'_1, \chi'_2, \hat{\mathbf{n}}_1 \cdot \hat{\mathbf{n}}_2) \equiv \langle [1 + \delta_{\text{tot}}(\tau_0 - \chi'_1, \chi'_1 \hat{\mathbf{n}}_1)] [1 + \delta_{\text{tot}}(\tau_0 - \chi'_2, \chi'_2 \hat{\mathbf{n}}_2)] \rangle, \quad (32)$$

where  $p_{\text{tot}}$  is given by Eq. (10), in which the density weighting (9) is now with respect to  $\delta_{\text{tot}}$  (instead of  $\delta$ ). In particular, notice that  $\xi_{\text{tot}}$  no longer depends on the separation  $r$ , as was the case before, but on the full triangular configuration given by three numbers, namely the side lengths  $\chi'_1, \chi'_2$ , and the opening angle  $\hat{\mathbf{n}}_1 \cdot \hat{\mathbf{n}}_2$ . As we will see in Sec. IV, this is because in a perturbative expansion  $\delta_{\text{tot}}$  contains terms depending on the line of

sight  $\hat{\mathbf{n}}$ , whose presence induces an angular dependence in the correlations, breaking statistical isotropy.

We can also see that the correlation function (32) is a function of the (apparent) past light cone: it manifestly expresses the unequal-time correlation of any two points  $S_1 = (\tau_1, \mathbf{s}_1) = (\tau_0 - \chi_1, \chi_1 \hat{\mathbf{n}}_1)$  and  $S_2 = (\tau_2, \mathbf{s}_2) = (\tau_0 - \chi_2, \chi_2 \hat{\mathbf{n}}_2)$ . As with our earlier Eq. (11), the formula we have just derived is still “summing over triangles,” but now the “triangles” are all those configurations that can be formed on the past light cone from an opening angle  $\hat{\mathbf{n}}_1 \cdot \hat{\mathbf{n}}_2$ , as opposed to those formed on spatial hypersurfaces. Since these configurations are on the light cone, they are in principle all observationally accessible, e.g. if the peculiar velocity of each galaxy was perfectly known. Hence the correlation function (32) is determined by marginalizing over all potentially observable configurations, unlike our earlier Eq. (11), which is determined by marginalizing over unobservable configurations.

Finally,  $\xi_s$  is expressed in terms of radial distances (assuming perfect knowledge of the underlying background cosmology), but we note that it is also possible, and perhaps more desirable, to express it in terms of observed and background redshifts,  $z$  and  $\bar{z}$ . Working in terms of redshifts and angles, the natural observable is the three-dimensional angular power spectrum  $C_\ell(z, z')$  [8,21], which we note can be constructed from our  $\xi_s$  if we leave arbitrary the conversion of redshift to distance.<sup>5</sup>

#### IV. RECOVERING LINEAR THEORY

We now verify that our nonlinear expression (31) of the redshift-space overdensity recovers well-known results from linear theory. To begin, we expand the last exponential in Eq. (31), keeping only up to the linear contribution in  $u_{\parallel}$ :

$$\begin{aligned} 1 + \delta_s(\tau, \chi \hat{\mathbf{n}}) &\simeq \frac{1}{\chi^2} \int d\chi' \chi'^2 [1 + \delta_{\text{tot}}(\tau', \chi' \hat{\mathbf{n}})] \\ &\quad \times \int \frac{d\mathbf{k}}{2\pi} e^{-ik(\chi - \chi')} (1 + iku_{\parallel}(\tau', \chi' \hat{\mathbf{n}})) \\ &= \frac{1}{\chi^2} \int d\chi' \chi'^2 [1 + \delta_{\text{tot}}(\tau', \chi' \hat{\mathbf{n}})] \\ &\quad \times \left( \delta_{\text{D}}(\chi - \chi') - u_{\parallel}(\tau', \chi' \hat{\mathbf{n}}) \frac{d}{d\chi} \delta_{\text{D}}(\chi - \chi') \right), \end{aligned} \quad (33)$$

where we have written factors of  $k$  as radial derivatives using  $ike^{-ik\chi} = -de^{-ik\chi}/d\chi$ . Note that in Eq. (33) we have made explicit the dependence of the field in the position  $\mathbf{x} = \chi' \hat{\mathbf{n}}$  but also in time  $\tau' = \tau_0 - \chi'$ , since the density and

velocity are evolving with time. Dropping the quadratic term  $u_{\parallel} \delta$ , taking the  $\chi$  derivative outside of the integral and calculating the now trivial integrals, we find (recalling that  $u_{\parallel} \equiv \mathcal{H}^{-1} v_{\parallel}$ )

$$\begin{aligned} 1 + \delta_s(\tau, \chi \hat{\mathbf{n}}) &= 1 + \delta_{\text{tot}}(\tau, \chi \hat{\mathbf{n}}) - \frac{1}{\chi^2} \frac{d}{d\chi} \left( \chi^2 \frac{v_{\parallel}(\tau, \chi \hat{\mathbf{n}})}{\mathcal{H}(\tau)} \right) \\ &= 1 + \delta_{\text{tot}}(\tau, \chi \hat{\mathbf{n}}) - \frac{1}{\chi^2} \frac{\partial}{\partial \chi} \left( \chi^2 \frac{v_{\parallel}(\tau, \chi \hat{\mathbf{n}})}{\mathcal{H}(\tau)} \right) \\ &\quad - \frac{1}{\chi^2} \frac{d\tau}{d\chi} \frac{\partial}{\partial \tau} \left( \chi^2 \frac{v_{\parallel}(\tau, \chi \hat{\mathbf{n}})}{\mathcal{H}(\tau)} \right) \\ &= 1 + \delta_{\text{tot}}(\tau, \chi \hat{\mathbf{n}}) - \frac{1}{\mathcal{H}} \frac{\partial v_{\parallel}}{\partial \chi} - \left( \frac{2}{\mathcal{H}\chi} + \frac{\dot{\mathcal{H}}}{\mathcal{H}^2} \right) v_{\parallel} \\ &\quad + \frac{1}{\mathcal{H}} \dot{v}_{\parallel}, \end{aligned} \quad (34)$$

where  $\tau = \tau_0 - \chi$  and an overdot denotes partial differentiation with respect to conformal time. Note that the second and third term in the second line is equal to  $\delta_s = \delta_{\text{tot}} - \nabla \cdot \mathbf{u}_{\parallel}$  [with the radial velocity field  $\mathbf{u}_{\parallel} \equiv \hat{\mathbf{n}} \cdot \mathbf{u}(\mathbf{x}) \hat{\mathbf{n}}$ ], a formula that is conventionally obtained by linearizing the Jacobian of the mapping (1). The last two terms in the last line of Eq. (34) arise because of the lookback time, and are thus not captured by the Jacobian.

The kinematic terms in Eq. (34) can be understood as follows. The third term, the radial derivative of the velocity, gives the well-known RSD effect. The fourth term, proportional to  $2/(\mathcal{H}\chi)$ , is the wide-angle contribution from a uniform selection function, already present in the original Kaiser formula. This term is usually ignored since at large distances (compared to the separation) it is subdominant to the standard RSD term, but it is important to include in a wide-angle analysis [35]. Less well known are the last two terms in Eq. (34); these are due to the fact that, because we are integrating along the line of sight, we are traversing a geodesic on the past light cone, with both  $\mathcal{H}$  and  $v_{\parallel}$  evolving along it [12].

In addition to these terms, which derive from the mapping itself, there are also the selection and evolution effects. These are contained in  $\delta_{\text{tot}}$ , Eq. (30), which at linear order reads  $\delta_{\text{tot}} \simeq \delta + \delta_{\text{evol}} + \delta_L + \delta_*$ . We calculate  $\delta_{\text{evol}}$ ,  $\delta_L$ , and  $\delta_*$  as follows.

- (i) For  $\delta_{\text{evol}}$ , expand  $F_{\text{evol}}(\tau')$  in Eq. (27) about  $\tau = \tau' + \delta\tau$ :

$$\begin{aligned} F_{\text{evol}}(\tau') &\simeq F_{\text{evol}}(\tau) - \frac{dF_{\text{evol}}}{d\tau} \delta\tau \\ &= F_{\text{evol}}(\tau) (1 - f_{\text{evol}} \mathcal{H} \delta\tau), \end{aligned} \quad (35)$$

where in the second equality the derivative has been evaluated using Eq. (16). Inserting this into

<sup>5</sup>See Refs. [32–34] for related work on connecting  $C_\ell(z, z')$  to the idealized power spectrum  $P(k)$ , corrected for unequal-time correlations and wide-angle effects.



Eq. (27) and using that by Eqs. (14) and (1)  $\delta\tau = -\delta\chi = -\mathcal{H}^{-1}v_{\parallel}$ , we find

$$\delta_{\text{evol}} = f_{\text{evol}}v_{\parallel}. \quad (36)$$

- (ii) For  $\delta_L$ , expand  $\bar{n}(\tau, L > \bar{L}_*(\chi'))$  in Eq. (28) around  $\chi = \chi' + \delta\chi$ . At linear order,

$$\begin{aligned} \bar{n}(\tau, L > \bar{L}_*(\chi')) &\simeq \bar{n}(\tau, L > \bar{L}_*(\chi)) \\ &\times \left( 1 - \frac{\partial \ln \bar{n}}{\partial \ln \bar{L}_*} \frac{d \ln \bar{L}_*}{d \ln \chi} \frac{\delta\chi}{\chi} \right), \end{aligned} \quad (37)$$

where all quantities on the right-hand side are evaluated at  $\chi$  and the chain rule has been used on the second term. Here  $\delta\chi = \mathcal{H}^{-1}v_{\parallel}$  and the  $\chi$  derivative is

$$\frac{d \ln \bar{L}_*}{d \ln \chi} = 2 \frac{d \ln \bar{d}_L}{d \ln \chi} = 2\mathcal{H}\chi \left( 1 + \frac{1}{\mathcal{H}\chi} \right), \quad (38)$$

where the first equality follows because  $\bar{L}_* \propto \bar{d}_L^2$  and the second equality follows from differentiating  $\bar{d}_L(\chi) = (1+z)\chi = \chi/a[\tau(\chi)]$ . Inserting the linear expansion (37) into Eq. (28), we have

$$\delta_L = 5s_* \left( 1 + \frac{1}{\mathcal{H}\chi} \right) v_{\parallel}, \quad (39)$$

where we have inserted Eq. (15) for the magnification bias, replacing  $\bar{n}$  with  $\bar{n}_s$  (since the difference results in a second-order correction).

- (iii) For  $\delta_*$ , expand  $\bar{n}(\tau', L > L_*(\mathbf{x}))$  in Eq. (28) around  $\bar{L}_*(\chi') = L_*(\mathbf{x}) - \delta L_*(\chi', \hat{\mathbf{n}})$ . At linear order,

$$\begin{aligned} \bar{n}(\tau', L > L_*(\mathbf{x})) &\simeq \bar{n}(\tau', L > \bar{L}_*(\chi')) \\ &\times \left( 1 + \frac{\partial \ln \bar{n}}{\partial \ln \bar{L}_*} \frac{\delta L_*(\chi', \hat{\mathbf{n}})}{\bar{L}_*(\chi')} \right). \end{aligned} \quad (40)$$

The perturbation to the threshold at a fixed position in real space is

$$\frac{\delta L_*(\chi', \hat{\mathbf{n}})}{\bar{L}_*(\chi')} = 2 \frac{\delta d_L(\chi', \hat{\mathbf{n}})}{\bar{d}_L(\chi')} = 4v_{\parallel}, \quad (41)$$

where the first equality follows from linearizing Eq. (25), while in the second equality we have used the luminosity distance fluctuations due to the source velocity calculated in Ref. [36].<sup>6</sup> Inserting the linear expansion (40) into Eq. (24), we obtain

$$\delta_* = -10s_*v_{\parallel}, \quad (42)$$

where again we have substituted in Eq. (15) for the magnification bias.

Finally, inserting Eqs. (36), (39), and (42) into Eq. (34) for  $\delta_{\text{tot}}$ , we obtain

$$\begin{aligned} \delta_s(\tau, \chi \hat{\mathbf{n}}) &= \delta - \frac{1}{\mathcal{H}} \frac{\partial v_{\parallel}}{\partial \chi} + \frac{1}{\mathcal{H}} \dot{v}_{\parallel} \\ &+ \left( f_{\text{evol}} - 5s_* - \frac{\dot{\mathcal{H}}}{\mathcal{H}^2} + \frac{5s_* - 2}{\mathcal{H}\chi} \right) v_{\parallel}. \end{aligned} \quad (43)$$

Upon comparing this equation with the full expression obtained from relativistic calculations—e.g. equation (2.13) in Ref. [37]—we see that we have recovered all subleading effects at  $\mathcal{O}(\mathcal{H}/k)$ , with the exception of two terms. The first is a kinematic term given simply as  $v_{\parallel}$ . This missing term can be traced back to the starting point of our derivation, Eq. (2), which is based on the naive Euclidean volume element  $d^3\mathbf{x}$ . This Newtonian derivation does not account for the fact that the hypersurface of constant time for the moving galaxies (in real space) does not coincide with the hypersurface of constant conformal time  $\tau$ . That is, these two frames are “tilted” with respect to one another, and it is by accounting for this that we recover precisely the term that we are after. From an observational point of view, this term arises because photons, followed back down the past light cone, do not probe the rest-frame galaxy density. Based on purely kinematic considerations, these photons will intercept more galaxies moving toward them versus away from them [38], so that if a galaxy is receding away from the observer then the apparent local density is enhanced relative to its intrinsic value. Technically speaking, the missing term arises through projection of the four-current  $j^\mu = nu^\mu$  at the source position onto the covariant three-dimensional volume element (the three-form dual to the one-form  $dx^\mu$ ). Clearly this requires a relativistic treatment, beginning with a covariant notion of number conservation; this is however beyond the scope of this work.

The second term missing is  $\mathcal{H}^{-1}\partial\Psi/\partial\chi$ , the contribution from the gravitational redshift. This can be put down to the simple fact that the standard mapping (1) only accounts for the dominant Doppler shift and therefore ignores the subdominant contribution from the gravitational redshift. To illustrate the basic structure in a minimal model, we have neglected to include the gravitational redshift. However, adding this effect into the model is straightforward: by Eq. (13) we take  $\mathbf{s}(\mathbf{x}) \rightarrow \mathbf{s}(\mathbf{x}) - \mathcal{H}^{-1}\Psi(\mathbf{x})\hat{\mathbf{x}}$ ; see also Refs. [19,20]. A complete model including the gravitational redshift and the relativistic tilt will be presented in a forthcoming work.

<sup>6</sup>See Eq. (53) [or equivalently Eq. (55)] in Ref. [36], noting that  $\hat{\mathbf{n}}$  there is equal to  $-\hat{\mathbf{n}}$  here.

## V. GAUSSIAN STREAMING MODEL ON THE FULL SKY

The discussion up to now has been fairly general in that no assumptions have been placed on the statistics of the velocities that determine  $p(\boldsymbol{\chi} - \boldsymbol{\chi}')$  and therefore the correlation function. We now wish to specify these statistics by presenting a particular model of Eq. (32), namely, the full-sky version of the Gaussian streaming model [28], often used in configuration-space analyses [39–42]. We will however include the selection and evolution effects, which we recall are entirely contained in  $\delta_{\text{tot}}$ , Eq. (30). The lookback time is also included, which amounts to taking  $\tau' \rightarrow \tau_0 - \chi'$ .

We follow the usual procedure [16,26] for constructing such models, namely, we rewrite the generating function  $Z$  in terms of the connected moments using the cumulant generating function  $W \equiv \ln Z$ , then Taylor expand  $W$ , keeping only the first and second connected moments (as determines a Gaussian). In detail, by expanding  $W(\mathbf{J}) \equiv \ln Z(\mathbf{J})$  about  $\mathbf{J} = 0$  we have

$$W(\mathbf{J}) = \sum_{n=1}^{\infty} \frac{i^n}{n!} J_{i_1} \cdots J_{i_n} \langle w_{i_1} \cdots w_{i_n} \rangle_{\delta_{\text{tot}}, \mathbf{c}},$$

$$\langle w_{i_1} \cdots w_{i_n} \rangle_{\delta_{\text{tot}}, \mathbf{c}} = (-i)^n \left. \frac{\partial^n \ln Z}{\partial J_{i_1} \cdots \partial J_{i_n}} \right|_{\mathbf{J}=0}, \quad (44)$$

where repeated indices are summed over, and  $i_1 = 1, 2, i_2 = 1, 2$ , etc. Here subscript  $\delta_{\text{tot}}$  denotes the density-weighted average (9), subscript “c” denotes the connected part of the moment, and  $w_i = u_{\parallel}(\tau_i, \mathbf{x}_i) = \hat{\mathbf{n}}_i \cdot \mathbf{u}(\tau_i, \mathbf{x}_i)$ . (Without loss of generality one may take the lines of sight  $\hat{\mathbf{n}}_1$  and  $\hat{\mathbf{n}}_2$  to lie within the  $xz$  plane, as in Fig. 1.) Then in terms of the connected moments

$$Z(\mathbf{J}) = \exp \left( \sum_{n=1}^{\infty} \frac{i^n}{n!} J_{i_1} \cdots J_{i_n} \langle w_{i_1} \cdots w_{i_n} \rangle_{\delta_{\text{tot}}, \mathbf{c}} \right). \quad (45)$$

These expressions are general. As mentioned, in the Gaussian streaming model we keep only the first and second connected moments, i.e. truncating the sum at  $n = 2$ . This leaves the mean and covariance,

$$\boldsymbol{\mu}(\chi'_1, \chi'_2, \hat{\mathbf{n}}_1 \cdot \hat{\mathbf{n}}_2) \equiv \langle \mathbf{w} \rangle_{\delta_{\text{tot}}, \mathbf{c}} = \begin{pmatrix} \langle u_{\parallel}(\chi'_1) \rangle_{\delta_{\text{tot}}, \mathbf{c}} \\ \langle u_{\parallel}(\chi'_2) \rangle_{\delta_{\text{tot}}, \mathbf{c}} \end{pmatrix}, \quad (46)$$

$$\mathbf{C}(\chi'_1, \chi'_2, \hat{\mathbf{n}}_1 \cdot \hat{\mathbf{n}}_2) \equiv \langle \mathbf{w} \mathbf{w}^T \rangle_{\delta_{\text{tot}}, \mathbf{c}} = \begin{pmatrix} \langle u_{\parallel}(\chi'_1) u_{\parallel}(\chi'_1) \rangle_{\delta_{\text{tot}}, \mathbf{c}} & \langle u_{\parallel}(\chi'_1) u_{\parallel}(\chi'_2) \rangle_{\delta_{\text{tot}}, \mathbf{c}} \\ \langle u_{\parallel}(\chi'_1) u_{\parallel}(\chi'_2) \rangle_{\delta_{\text{tot}}, \mathbf{c}} & \langle u_{\parallel}(\chi'_2) u_{\parallel}(\chi'_2) \rangle_{\delta_{\text{tot}}, \mathbf{c}} \end{pmatrix}. \quad (47)$$

Here we have used the shorthand  $u_{\parallel}(\chi'_i) \equiv u_{\parallel}(\tau_0 - \chi'_i, \chi'_i \hat{\mathbf{n}}_i)$ . Note that the mean radial velocity  $\boldsymbol{\mu}$ , being density weighted,

does not in general vanish. Keeping terms in Eq. (45) up to second order in  $\mathbf{J}$  yields the generating function of a Gaussian:

$$Z(\mathbf{J}) = \exp \left( i \mathbf{J} \cdot \boldsymbol{\mu} - \frac{1}{2} \mathbf{J}^T \mathbf{C} \mathbf{J} \right). \quad (48)$$

Inverse Fourier transform of  $Z(\mathbf{J})$ , i.e. evaluating Eq. (10), thus yields a two-dimensional Gaussian with mean  $\boldsymbol{\mu}$  and covariance  $\mathbf{C}$ , which when inserted back into Eq. (32) furnishes the wide-angle Gaussian streaming model,<sup>7</sup>

$$1 + \xi_s(\chi_1, \chi_2, \hat{\mathbf{n}}_1 \cdot \hat{\mathbf{n}}_2) = \frac{1}{\chi_1^2 \chi_2^2} \int_0^{\infty} d\chi'_1 \chi_1'^2 \int_0^{\infty} d\chi'_2 \chi_2'^2 [1 + \xi_{\text{tot}}(\chi'_1, \chi'_2, \hat{\mathbf{n}}_1 \cdot \hat{\mathbf{n}}_2)] \times \frac{1}{2\pi |\mathbf{C}|^{1/2}} \exp \left( -\frac{1}{2} (\boldsymbol{\chi} - \boldsymbol{\chi}' - \boldsymbol{\mu})^T \mathbf{C}^{-1} (\boldsymbol{\chi} - \boldsymbol{\chi}' - \boldsymbol{\mu}) \right), \quad (49)$$

remembering that  $\boldsymbol{\mu}$  and  $\mathbf{C}$  are functions of  $\chi'_1, \chi'_2$ , and  $\hat{\mathbf{n}}_1 \cdot \hat{\mathbf{n}}_2$ . Note that this model does not assume that  $\delta$  and  $u_{\parallel}$  are Gaussian fields, nor is it assuming that in the perturbative expansion (48) the fields  $\delta$  and  $u_{\parallel}$  are small fluctuations. Rather, this model is based on the *correlations* being small on large scales. The Gaussian distribution arises from our having truncated the generating function at second order in  $\mathbf{J} = \boldsymbol{\kappa}$ . Of course, extensions to Eq. (49) to include higher-order, non-Gaussian statistics are also possible [43].

The equivalent model without selection and evolution effects is obtained by taking  $\xi_{\text{tot}} \rightarrow \xi$  and  $\delta_{\text{tot}} \rightarrow \delta$  in the density weighting. The above model also takes into account the lookback time, which can be ignored by treating time in the usual way, i.e. as an independent variable (not degenerate with distance). Overall, the effect of these three effects changes the quantitative predictions but does not change the basic form of the model.

Equation (49) is the full-sky generalization of the well-known Gaussian streaming model of the distant-observer limit:

$$1 + \xi_s(s, \boldsymbol{\mu}) = \int_{-\infty}^{\infty} dr_{\parallel} [1 + \xi(r)] \cdot \frac{1}{\sqrt{2\pi} \sigma_{12}(\mathbf{r})} \times \exp \left( -\frac{1}{2} \frac{(s_{\parallel} - r_{\parallel} - u_{12}(\mathbf{r}))^2}{\sigma_{12}^2(\mathbf{r})} \right), \quad (50)$$

where  $r_{\parallel}$  and  $s_{\parallel}$  are the real- and redshift-space separations along the line of sight, and  $u_{12}(\mathbf{r}) \equiv \langle \Delta u_{\parallel} \rangle_{\delta_{\text{tot}}, \mathbf{c}}$  and  $\sigma_{12}^2(\mathbf{r}) \equiv \langle (\Delta u_{\parallel})^2 \rangle_{\delta_{\text{tot}}, \mathbf{c}}$ , where  $\Delta u_{\parallel} \equiv \hat{\mathbf{n}} \cdot \mathbf{u}(\mathbf{x}_1) - \hat{\mathbf{n}} \cdot \mathbf{u}(\mathbf{x}_2)$ , are the

<sup>7</sup>Since we are using spherical coordinates, the probability distribution is perhaps better described as a Maxwell-Boltzmann distribution  $p \propto x^2 e^{-x^2}$  (or some two-dimensional analog thereof). Although for large variance we note that the Maxwellian is well approximated by a Gaussian (in the one-dimensional case).

mean and dispersion of the pairwise velocity, respectively, and all quantities are evaluated at a fixed time. Although the wide-angle and distant-observer models are similar in form, it requires some work to show that Eq. (49) does indeed reduce to Eq. (50) in the appropriate limit. We leave the details of this calculation to Appendix B.

## VI. MULTIPOLE EXPANSION IN THE WIDE-ANGLE REGIME

In this section we show that Eq. (11) recovers the standard linear predictions for the multipoles, including those induced when going beyond the distant-observer limit. Since the aim here is to compare our results with those in the wide-angle literature, we will ignore contributions from galaxy evolution and relativistic effects.

To facilitate the calculation, recall that the correlation function on a fixed redshift slice can be expanded about the distant-observer limit as [44]

$$\xi_s(s, \mu, d) = \sum_{n=0}^{\infty} \left(\frac{s}{d}\right)^n \sum_{\ell=0}^{\infty} \xi_{\ell}^{(n)}(s, d) \mathcal{L}_{\ell}(\mu), \quad (51)$$

i.e. in terms of a small expansion parameter  $\epsilon \equiv s/d$ , where for closely separated lines of sight a low-order expansion is valid. Here  $\mathcal{L}_{\ell}$  is a Legendre polynomial of the  $\ell$ th degree,  $s = |\mathbf{s}_1 - \mathbf{s}_2|$  is the separation,  $\mu = \cos \theta$  (see Fig. 1), and  $d$  is some distance to the galaxy pair (to be made precise shortly). Note that in addition to the explicit dependence of the multipoles in  $d$  via  $\epsilon$ ,  $\xi_{\ell}^{(n)}$  depends also on  $d$  through the evolution of the density and velocity, which depend on redshift, and therefore varies with distance  $d$ . The usual Kaiser multipoles [3] are given by the  $n = 0$  multipoles:

$$\xi_0^{(0)}(s) = \int \frac{k^2 dk}{2\pi^2} j_0(ks) \left( b_A b_B P_{\delta\delta}(k) - \frac{1}{3}(b_A + b_B) P_{\theta\delta}(k) + \frac{1}{5} P_{\theta\theta}(k) \right), \quad (52a)$$

$$\xi_2^{(0)}(s) = \int \frac{k^2 dk}{2\pi^2} j_2(ks) \left( \frac{2}{3}(b_A + b_B) P_{\theta\delta}(k) - \frac{4}{7} P_{\theta\theta}(k) \right), \quad (52b)$$

$$\xi_4^{(0)}(s) = \int \frac{k^2 dk}{2\pi^2} j_4(ks) \frac{8}{35} P_{\theta\theta}(k), \quad (52c)$$

where  $b_A$  and  $b_B$  are the linear galaxy bias of two tracers labeled A and B, and  $\theta = -f\delta$ , where  $f$  is the growth rate. The wide-angle corrections are given by multipoles  $n \geq 1$ , and the  $\ell$ th multipole is given by the sum  $\xi_{\ell}(s, d) \equiv \sum_n \epsilon^n \xi_{\ell}^{(n)}(s, d)$ . Unlike in the distant-observer limit, the wide-angle contributions to the multipoles depend on how the angular separation  $\mu$  is defined, i.e. what we choose for the line of sight [14,44].

## A. Midpoint parametrization

The shape and size of the multipoles depend on how we parametrize the triangle as formed by the galaxy pair with the observer. In particular, we need to fix the definition of  $\mu$ . This means choosing a line of sight, and there is no unique choice for this. In this work we use the line of sight defined by the midpoint parametrization (see Fig. 1). This section describes this parametrization and collects some useful formulas. In Appendix D we give a formula relating multipoles in the midpoint parametrization to those in the end-point parametrization.

First, the midpoint of the separation  $\mathbf{s} = \mathbf{s}_1 - \mathbf{s}_2$  is given by  $\mathbf{d} \equiv (\mathbf{s}_1 + \mathbf{s}_2)/2$ . We thus have  $\mathbf{s}_1 = \mathbf{d} + \mathbf{s}/2$  and  $\mathbf{s}_2 = \mathbf{d} - \mathbf{s}/2$ . The expansion parameter in Eq. (51) is  $\epsilon \equiv s/d$ . In particular, we may align  $\mathbf{d}$  with the  $+z$  axis, i.e.  $\hat{\mathbf{d}} = \mathbf{e}_z$ . We can also without loss of generality place the triangular configuration in the  $xz$  plane, with the first galaxy placed in the left half-plane (with negative  $x$  coordinate) and the second galaxy placed in the right half-plane (with positive  $x$  coordinate); see Fig. 1. With these choices  $\hat{\mathbf{s}} = -\sqrt{1-\mu^2}\mathbf{e}_x + \mu\mathbf{e}_z$ , with  $\mu \equiv \mathbf{e}_z \cdot \hat{\mathbf{s}}$  and  $\mathbf{e}_x, \mathbf{e}_z$  are unit vectors along the  $x$  and  $z$  axes, respectively. Now  $\mathbf{s}_1 = d(\mathbf{e}_z + \epsilon\hat{\mathbf{s}}/2)$  and  $\mathbf{s}_2 = d(\mathbf{e}_z - \epsilon\hat{\mathbf{s}}/2)$ , from which the unit vectors are found to be

$$\begin{aligned} \hat{\mathbf{n}}_1 \equiv \hat{\mathbf{s}}_1 &= \left( \mathbf{e}_z + \frac{\epsilon}{2}\hat{\mathbf{s}} \right) \sum_{n=0}^{\infty} \left( -\frac{\epsilon}{2} \right)^n \mathcal{L}_n(\mu) \\ &= \mathbf{e}_z - \frac{\epsilon}{2}\sqrt{1-\mu^2}\mathbf{e}_x + \mathcal{O}(\epsilon^2), \end{aligned} \quad (53a)$$

$$\begin{aligned} \hat{\mathbf{n}}_2 \equiv \hat{\mathbf{s}}_2 &= \left( \mathbf{e}_z - \frac{\epsilon}{2}\hat{\mathbf{s}} \right) \sum_{n=0}^{\infty} \left( +\frac{\epsilon}{2} \right)^n \mathcal{L}_n(\mu) \\ &= \mathbf{e}_z + \frac{\epsilon}{2}\sqrt{1-\mu^2}\mathbf{e}_x + \mathcal{O}(\epsilon^2). \end{aligned} \quad (53b)$$

Observe that at  $\mathcal{O}(\epsilon)$ , the lines of sight  $\hat{\mathbf{n}}_1$  and  $\hat{\mathbf{n}}_2$  are symmetric about the  $z$  axis (equal and opposite  $x$  components).

Note the following relations when going between variables  $\{\chi_1, \chi_2, \cos \vartheta \equiv \hat{\mathbf{n}}_1 \cdot \hat{\mathbf{n}}_2\}$  and  $\{s, d, \mu\}$ :  $s = (\chi_1^2 + \chi_2^2 - 2\chi_1\chi_2 \cos \vartheta)^{1/2}$ ,  $d = \frac{1}{2}(\chi_1^2 + \chi_2^2 + 2\chi_1\chi_2 \cos \vartheta)^{1/2}$ , and  $\mu^2 = \frac{1}{4}(\chi_1^2 - \chi_2^2)^2 / [(\chi_1^2 + \chi_2^2)^2 - (2\chi_1\chi_2 \cos \vartheta)^2]$ . These follow from the cosine rule.

## B. Linear theory

We now show that Eq. (7) recovers at zeroth order ( $n = 0$ ) the standard Kaiser multipoles [3], and at the first order ( $n = 1$ ) the wide-angle corrections. As mentioned, the wide-angle corrections vanish at first order in the auto-correlation function but not for the cross-correlation function. We will thus consider the cross-correlation between two tracer populations, described by linear bias  $b_A$  and  $b_B$ . We will assume no magnification and evolution bias since

we have already shown in Sec. IV that we recover the correct linear expression for  $\delta_s$ . The details of our computations can be found in Appendix C.

First we convert Eq. (7) to the cross-correlation. In linear theory this is done simply by replacing  $\delta(\mathbf{x}_1) \rightarrow b_A \delta(\mathbf{x}_1)$  and  $\delta(\mathbf{x}_2) \rightarrow b_B \delta(\mathbf{x}_2)$ :

$$1 + \xi_s(s, \mu, d) = \frac{1}{\chi_1^2 \chi_2^2} \int d\chi'_1 \chi_1'^2 \int d\chi'_2 \chi_2'^2 \int \frac{d^2\boldsymbol{\kappa}}{(2\pi)^2} e^{-i\boldsymbol{\kappa} \cdot (\boldsymbol{\chi} - \boldsymbol{\chi}')} \times \langle (1 + b_A \delta_1)(1 + b_B \delta_2) e^{i\boldsymbol{\kappa} \cdot \mathbf{w}} \rangle. \quad (54)$$

Here we have used the shorthand  $\delta_1 = \delta(\mathbf{x}_1)$  and  $\delta_2 = \delta(\mathbf{x}_2)$ , and as before  $\mathbf{w} = (u_{\parallel}(\mathbf{x}_1), u_{\parallel}(\mathbf{x}_2))$ . For convenience we will also write

$$U_i(\mathbf{r}) = \langle u_i(\mathbf{x}_1) \delta(\mathbf{x}_2) \rangle \quad \text{and} \quad \Psi_{ij}(\mathbf{r}) = \langle u_i(\mathbf{x}_1) u_j(\mathbf{x}_2) \rangle \quad (55)$$

for the velocity-density and velocity-velocity correlation functions. Here the separation  $\mathbf{r} = \mathbf{x}_1 - \mathbf{x}_2$  is given in terms of the radial distances as  $\mathbf{r}(\boldsymbol{\chi}') = \chi'_1 \hat{\mathbf{n}}_1 - \chi'_2 \hat{\mathbf{n}}_2$ , and in redshift space  $\mathbf{s}(\boldsymbol{\chi}) = \chi_1 \hat{\mathbf{n}}_1 - \chi_2 \hat{\mathbf{n}}_2 = \mathbf{r}(\boldsymbol{\chi})$ .

The idea of the calculation is to expand  $e^{i\boldsymbol{\kappa} \cdot \mathbf{w}}$ , keeping up to quadratic terms and dropping zero-lag terms (which are absent in the linear predictions). The integrations can then be done analytically (see Appendix C for details). The result is

$$\begin{aligned} \xi_s(\chi_1, \chi_2, \hat{\mathbf{n}}_1 \cdot \hat{\mathbf{n}}_2) &= b_A b_B \xi(s) - b_B \frac{\partial}{\partial \chi_1} U_i \hat{n}_1^i + b_A \frac{\partial}{\partial \chi_2} U_i \hat{n}_2^i \\ &\quad + \frac{\partial}{\partial \chi_1} \frac{\partial}{\partial \chi_2} \Psi_{ij} \hat{n}_1^i \hat{n}_2^j - b_B \frac{2}{\chi_1} U_i \hat{n}_1^i \\ &\quad + b_A \frac{2}{\chi_2} U_i \hat{n}_2^i + \left( \frac{2}{\chi_1} \frac{\partial}{\partial \chi_2} + \frac{2}{\chi_2} \frac{\partial}{\partial \chi_1} \right) \Psi_{ij} \hat{n}_1^i \hat{n}_2^j. \end{aligned} \quad (56)$$

This is the linear correlation function corresponding to the right-hand side of Eq. (34). Here  $\xi$ ,  $U_i$ , and  $\Psi_{ij}$  depend on  $\chi_1$  and  $\chi_2$  through  $\mathbf{s}$  (and we remember that lines of sight are always constant with respect to their radial derivatives,  $\partial \hat{n}^i / \partial \chi = 0$ ). The first line in Eq. (56) yields the usual Kaiser multipoles (among wide-angle corrections), while the second line consists of terms suppressed by a factor of  $\mathcal{H}/k$  with respect to the Kaiser multipoles, but are of the same order as the wide-angle contributions.

### 1. Distant-observer limit

The multipoles of the distant-observer limit (i.e. the Kaiser multipoles) can be recovered by setting  $\hat{\mathbf{n}}_1 = \hat{\mathbf{n}}_2 = \mathbf{e}_z = (0, 0, 1)$  and taking  $\chi_1, \chi_2 \rightarrow \infty$ . Doing so eliminates the second line of terms in Eq. (56), leaving

$$\xi_s(s, \mu) = b_A b_B \xi(s) - (b_A + b_B) \partial_3 U_3(s, \mu) - \partial_3^2 \Psi_{33}(s, \mu) \quad (\text{distant-observer limit}) \quad (57)$$

where derivatives are with respect to  $s_3$ , the  $z$  component of  $\mathbf{s}$ . This equation was first derived in Ref. [45]. A straightforward computation of the derivatives yields

$$\partial_3 U_3(s, \mu) = \int \frac{k^2 dk}{2\pi^2} \left( \frac{1}{3} j_0(ks) - \frac{2}{3} j_2(ks) \mathcal{L}_2(\mu) \right) P_{\theta\delta}(k), \quad (58a)$$

$$\begin{aligned} \partial_3^2 \Psi_{33}(s, \mu) &= - \int \frac{k^2 dk}{2\pi^2} \left( \frac{1}{5} j_0(ks) - \frac{4}{7} j_2(ks) \mathcal{L}_2(\mu) \right. \\ &\quad \left. + \frac{8}{35} j_4(ks) \mathcal{L}_4(\mu) \right) P_{\theta\theta}(k), \end{aligned} \quad (58b)$$

where  $j_\ell$  is the  $\ell$ -th-order spherical Bessel function. From here it is not difficult to assemble the Kaiser multipoles (52).

### 2. Wide-angle corrections

The wide-angle corrections enter the  $U_i$  terms at order  $\epsilon$  and the  $\Psi_{ij}$  terms at  $\epsilon^2$ . (Note that in the autocorrelation, i.e. when  $b_A = b_B$ , the corrections also enter  $U_i$  at  $\epsilon^2$ .) Since we are interested only in the leading-order corrections (order  $\epsilon$ ), we need only focus on terms involving  $U_i$  in Eq. (56); the terms involving  $\Psi_{ij}$  are as given in the distant-observer limit so require no further calculation. For the  $\partial_i U_j$  terms in the first line of Eq. (56), we have

$$\begin{aligned} &- b_B \frac{\partial}{\partial \chi_1} U_i \hat{n}_1^i + b_A \frac{\partial}{\partial \chi_2} U_i \hat{n}_2^i \\ &= -(b_A + b_B) \int \frac{k^2 dk}{2\pi^2} \left( \frac{1}{3} j_0(ks) - \frac{2}{3} j_2(ks) \mathcal{L}_2(\mu) \right) P_{\theta\delta}(k) \\ &\quad - \frac{2}{5} \epsilon (b_A - b_B) \int \frac{k^2 dk}{2\pi^2} (\mathcal{L}_1(\mu) - \mathcal{L}_3(\mu)) j_2(ks) P_{\theta\delta}(k), \end{aligned} \quad (59)$$

where the first integral on the right-hand side is the distant-observer contribution, and the second integral is the leading-order wide-angle correction.<sup>8</sup> The details of this computation can be found in Appendix C. For the  $U_i$  terms in Eq. (56) up to leading order in  $\epsilon$ , we have

$$\begin{aligned} &- b_B \frac{2}{\chi_1} U_i \hat{n}_1^i + b_A \frac{2}{\chi_2} U_i \hat{n}_2^i \\ &= 2\epsilon (b_A - b_B) \int \frac{k^2 dk}{2\pi^2} \frac{j_1(ks)}{ks} \mathcal{L}_1(\mu) P_{\theta\delta}(k). \end{aligned} \quad (60)$$

<sup>8</sup>This agrees with Eqs. (52) and (53) in Ref. [12]; see also Eq. (3.19) in Ref. [46].

The leading-order wide-angle multipoles are thus

$$\xi_1^{(1)}(s) = (b_A - b_B) \int \frac{k^2 dk}{2\pi^2} \left( -\frac{2}{5} j_2(ks) + 2 \frac{j_1(ks)}{ks} \right) P_{\theta\delta}(k), \quad (61a)$$

$$\xi_3^{(1)}(s) = \frac{2}{5} (b_A - b_B) \int \frac{k^2 dk}{2\pi^2} j_2(ks) P_{\theta\delta}(k). \quad (61b)$$

These are consistent with those given in, e.g. Refs. [18,46]. Note that when working within the end-point parametrization the odd multipoles,  $\xi_1^{(1)}$  and  $\xi_3^{(1)}$ , receive additional contributions, which are of a geometric, noncosmological nature (Appendix D). Thus we have recovered the linear multipoles.

## VII. CONCLUSIONS

We have described a framework to model in the nonlinear regime not only wide-angle effects but also selection and relativistic effects. Our main result is Eq. (32), an expression for the redshift-space correlation function which is valid in both the nonlinear regime and on the full sky, accounts for the survey flux limit and the population evolution of tracers. Based on this expression, we have also given the full-sky generalization of the Gaussian streaming model, Eq. (49), which we have checked reduces to the well-known flat-sky model (50) in the appropriate limit.

The correlation function (32) takes a lensing-like form (i.e. is given by integrals along each line of sight) which can be understood probabilistically: a given two-point correlation in redshift space is determined by averaging over all the possible two-point correlations in real space that can be formed on the two lines of sight. Geometrically, this can be understood as a weighted sum over the space of triangular configurations in which the observer is fixed at one vertex with the galaxies at the other two (at the ends of the lines of sight). Since the opening angle is fixed, the probability space is two dimensional and given by the joint statistics of the line-of-sight components of the galaxy velocities. We note that this heuristic generalizes to higher-order correlation functions (e.g. for the three-point function the sum is over tetrahedrons).

We have also given a nonperturbative expression (31) for the overdensity in redshift space. Performing a perturbative expansion of this expression, we showed that we are able to recover all but two terms of the well-known linear expression of the overdensity at subleading order; see Eq. (43). The first term missing traces back to the fact that observations probe the number density of galaxies not in their rest frame but in a frame tilted with respect to it. This results in an additional kinematic term but requires a covariant expression of number conservation. The second term is the gravitational redshift, whose absence is due to the simple

fact that we have chosen to exhibit the formalism using the familiar redshift mapping (1). A model of the overdensity, complete down to  $\mathcal{O}(\mathcal{H}/k)$  effects, will be presented in a follow-up work. Nevertheless, the expression we have derived provides a compact description of a large number of terms (RSD, magnification bias, evolution bias, projection effects related to the light cone, etc.). Furthermore, our work provides a simple quasi-Newtonian derivation to the full relativistic calculation.

In summary, we have shown that the streaming model is not limited to the distant-observer limit but that it can be straightforwardly extended into the wide-angle regime and be built upon to include a number of other important effects. In a future work we will present numerical results for a realistic model including nonlinear evolution and galaxy bias, with a view toward an eventual measurement of the gravitational redshift.

## ACKNOWLEDGMENTS

This work is supported by the European Research Council (ERC) under the European Union's Horizon 2020 research and innovation program (Grant Agreement No. 863929; project title "Testing the law of gravity with novel large-scale structure observables"). C. B. acknowledges support from the Swiss National Science Foundation.

## APPENDIX A: ON THE MEAN DENSITY IN THE WIDE-ANGLE REGIME

In Sec. II we assumed that  $\bar{n}_s \equiv \langle n_s(\mathbf{s}) \rangle = \bar{n}$ . However, this is not assured in the wide-angle regime. This can be shown by direct calculation of the expectation of Eq. (3):

$$\langle n_s(\mathbf{s}) \rangle = \frac{1}{\chi^2} \bar{n} \int_0^\infty d\chi' \chi'^2 \int \frac{dk}{2\pi} e^{-ik(\chi-\chi')} \langle [1 + \delta(\chi' \hat{\mathbf{n}})] e^{iku_{\parallel}} \rangle. \quad (A1)$$

In general, the right-hand side does *not* evaluate to  $\bar{n}$ . We can see this as follows. By the cumulant expansion formula  $\langle e^{iX} \rangle = \exp\langle e^{iX} \rangle_c$ , we have that  $\langle e^{iku_{\parallel}} \rangle = e^{-k^2 \sigma_u^2 / 2}$  and  $\langle e^{iku_{\parallel}} \delta \rangle = 0$ , assuming as a first approximation that  $\delta$  and  $u_{\parallel}$  are Gaussian fields. Recognizing that  $e^{-k^2 \sigma_u^2 / 2}$  is the Fourier transform of a Gaussian with mean zero and variance  $\sigma_u^2$ , we have

$$\langle n_s(\mathbf{s}) \rangle = \frac{1}{\chi^2} \bar{n} \int_0^\infty d\chi' \chi'^2 \frac{1}{\sqrt{2\pi}\sigma_u} e^{-(\chi-\chi')^2 / 2\sigma_u^2}. \quad (A2)$$

That the mean density  $\langle n_s(\mathbf{s}) \rangle$  is a position-dependent quantity may seem strange at first, but this is just a consequence of the loss of statistical homogeneity in the wide-angle regime, with the observer representing a preferred location in space. Indeed, in the distant-observer limit, where homogeneity is retained, this  $\chi$  dependence

drops out: if  $\chi \gg \sigma_u$ , then the Gaussian in the integrand is sharply peaked around  $\chi' = \chi$ , so that the integral evaluates to approximately  $\chi^2$ . Therefore  $\langle n_s \rangle \rightarrow \bar{n}$  as  $\chi/\sigma_u \rightarrow \infty$ , so that it is perfectly valid to take  $\langle n_s \rangle = \bar{n}$  in this limit. But short of this limit there are corrections, which decrease with depth. Fortunately, convergence to this limit is rapid. Quantitatively, with the  $\Lambda$ CDM value  $\sigma_u = 5.8h^{-1}$  Mpc (corresponding to a velocity dispersion of about  $300 \text{ km s}^{-1}$ ), we find for depths  $\chi \geq 100h^{-1}$  Mpc (or  $z \geq 0.023$ ) that the deviations from  $\langle n_s(\mathbf{s}) \rangle / \bar{n} = 1$  are  $\leq 0.3\%$ , i.e. small in most situations of interest.

There are of course corrections to these estimates from non-Gaussianity due to nonlinear gravitational evolution. These corrections are largest on small scales  $k \sim 1/\chi$ . On intermediate scales  $k \sim 0.1h \text{ Mpc}^{-1}$ , where nonlinearities begin to be important, we expect perturbatively small departures from Gaussianity. This translates to non-Gaussianities becoming important at depths  $\chi \simeq 60h^{-1}$  Mpc ( $z \sim 0.01$ ) or shallower, i.e. small or negligible by the time we reach the convergence scale  $\chi \simeq 100h^{-1}$  Mpc. This means that, unless one's sample contains very local galaxies, there seems little harm in taking  $\langle n_s(\mathbf{s}) \rangle = \bar{n}$  (though one can always include the corrections should they be wanted).

## APPENDIX B: RECOVERING THE STANDARD GAUSSIAN STREAMING MODEL OF THE DISTANT-OBSERVER LIMIT

In this appendix we verify that the usual distant-observer streaming model (50) is recovered as a special case of the full-sky streaming model (49). Clearly we must end up with one less integral, leaving an integral over the separation  $r_{\parallel}$ . However, this is not as straightforward as simply taking the distant-observer limit,  $\chi_1, \chi_2 \rightarrow \infty$  and  $\hat{\mathbf{n}}_1 \rightarrow \hat{\mathbf{n}}_2$ . It turns out to be convenient to center the coordinates on the redshift-space positions, with the coordinate transformation  $\chi'_1 = \chi_1 - q_1$  and  $\chi'_2 = \chi_2 - q_2$ , or  $\chi' = \chi - \mathbf{q}$ . Equation (49) then reads

$$\begin{aligned} & 1 + \xi_s(\chi_1, \chi_2, \hat{\mathbf{n}}_1 \cdot \hat{\mathbf{n}}_2) \\ &= \int_{-\infty}^{\chi_1} dq_1 \left(1 - \frac{q_1}{\chi_1}\right)^2 \int_{-\infty}^{\chi_2} dq_2 \left(1 - \frac{q_2}{\chi_2}\right)^2 [1 + \xi(r)] \\ & \quad \times \frac{1}{2\pi|\mathbf{C}(\mathbf{r})|^{1/2}} \exp\left(-\frac{1}{2}(\mathbf{q} - \boldsymbol{\mu}(\mathbf{r}))^T \mathbf{C}^{-1}(\mathbf{r})(\mathbf{q} - \boldsymbol{\mu}(\mathbf{r}))\right). \end{aligned} \quad (\text{B1})$$

(Here we have ignored for simplicity the selection effects and the lookback time so that  $\boldsymbol{\mu}$  and  $\mathbf{C}$  depend on a triangle configuration parametrized by  $\mathbf{r}$ , i.e. we are working on a constant-time hypersurface.) In the limit  $\chi_1, \chi_2 \rightarrow \infty$  the first two factors in parentheses tend to unity (noting that at large  $q_1, q_2$  these factors become irrelevant as the Gaussian rapidly takes the whole integrand to zero). Thus, setting

these factors to unity, and doing some straightforward matrix algebra, the foregoing expression becomes

$$\begin{aligned} 1 + \xi_s &= \int_{-\infty}^{\infty} dq_1 \int_{-\infty}^{\infty} dq_2 \frac{1 + \xi(r)}{2\pi\sigma^2\sqrt{1-\rho^2}} \\ & \quad \times \exp\left(-\frac{1}{2} \frac{(\Delta_1 - \Delta_2)^2 + 2(1-\rho)\Delta_1\Delta_2}{\sigma^2(1-\rho^2)}\right), \end{aligned} \quad (\text{B2})$$

where as shorthand  $\Delta_1 \equiv q_1 - \mu_1$  and  $\Delta_2 \equiv q_2 - \mu_2$ , while  $C_{11} = C_{22} = \sigma^2$  and  $C_{12} = \rho\sigma^2$ , where  $\sigma = \sigma(\mathbf{r})$  and  $\rho = \rho(\mathbf{r})$  (or functions of  $q_1$  and  $q_2$ ). Defining the line-of-sight separation in real and redshift space,  $r_{\parallel} = \chi'_1 - \chi'_2$  and  $s_{\parallel} = \chi_1 - \chi_2$ , and the midpoints  $\bar{r}_{\parallel} = (\chi'_1 + \chi'_2)/2$  and  $\bar{s}_{\parallel} = (\chi_1 + \chi_2)/2$ , we have  $q_1 - q_2 = s_{\parallel} - r_{\parallel}$  and  $(q_1 + q_2)/2 = \bar{s}_{\parallel} - \bar{r}_{\parallel}$ , which implies  $q_1 = \bar{s}_{\parallel} - \bar{r}_{\parallel} + \frac{1}{2}(s_{\parallel} - r_{\parallel})$  and  $q_2 = \bar{s}_{\parallel} - \bar{r}_{\parallel} - \frac{1}{2}(s_{\parallel} - r_{\parallel})$ . (Note that  $s_{\parallel}$  and  $\bar{s}_{\parallel}$  are fixed by the redshift-space configuration.) Making another change of coordinates,  $(q_1, q_2)$  to  $(r_{\parallel}, \bar{r}_{\parallel})$ , we have after some more algebra

$$\begin{aligned} 1 + \xi_s(s_{\parallel}, s_{\perp}) &= \int_{-\infty}^{\infty} dr_{\parallel} \frac{1 + \xi(r)}{2\pi\sigma^2\sqrt{1-\rho^2}} \\ & \quad \times \exp\left(-\frac{1}{2} \frac{(s_{\parallel} - r_{\parallel} - u_{12})^2}{2\sigma^2(1-\rho)}\right) \\ & \quad \times \int_{-\infty}^{\infty} d\bar{r}_{\parallel} \exp\left(-\frac{(\bar{s}_{\parallel} - \bar{r}_{\parallel})^2}{\sigma^2(1+\rho)}\right), \end{aligned} \quad (\text{B3})$$

where we recognized that  $\mu_1 - \mu_2 = \langle u_{\parallel}(\mathbf{x}_1) \rangle_{\delta,c} - \langle u_{\parallel}(\mathbf{x}_2) \rangle_{\delta,c} \equiv u_{12}$ , and noted that  $u_{12}$ ,  $\sigma$ , and  $\rho$  depend on  $r_{\parallel}$ , but not  $\bar{r}_{\parallel}$ , hence the last integral. Here we have  $r^2 = r_{\parallel}^2 + r_{\perp}^2$  and  $r_{\perp} = s_{\perp}$ . Upon doing the last (Gaussian) integral over  $\bar{r}_{\parallel}$  and noting that  $2\sigma^2(1-\rho) = 2C_{11} - 2C_{12} = \langle (\Delta u_{\parallel})^2 \rangle_{\delta,c} \equiv \sigma_{12}^2$ , we hence recover Eq. (50), the usual Gaussian streaming model, i.e. in the distant-observer limit.

## APPENDIX C: LINEAR THEORY MULTIPOLES

In this appendix we calculate the contributions to the multipoles from wide-angle effects and inverse-distance terms (from the selection function), filling in some of the details of Sec. VI B. We will compute from Eq. (11) the leading-order wide-angle corrections, i.e. at  $\mathcal{O}(\epsilon)$ , and will consider the cross-correlation of two different tracers, described by linear bias  $b_A$  and  $b_B$ . For this calculation it is convenient to start with Eq. (7), which for the cross-correlation function is given by simply replacing  $\delta(\mathbf{x}_1) \rightarrow b_A \delta(\mathbf{x}_1)$  and  $\delta(\mathbf{x}_2) \rightarrow b_B \delta(\mathbf{x}_2)$ :

$$1 + \xi_s(s, \mu, d) = \frac{1}{\chi_1^2 \chi_2^2} \int \chi_1'^2 d\chi_1' \int \chi_2'^2 d\chi_2' \int \frac{d^2 \boldsymbol{\kappa}}{(2\pi)^2} e^{-i\boldsymbol{\kappa} \cdot (\boldsymbol{x} - \boldsymbol{x}')} \times \langle (1 + b_A \delta_1)(1 + b_B \delta_2) e^{i\boldsymbol{\kappa} \cdot \mathbf{w}} \rangle. \quad (\text{C1})$$

Here we have used the shorthand  $\delta_1 = \delta(\mathbf{x}_1)$  and  $\delta_2 = \delta(\mathbf{x}_2)$ , and as before  $\mathbf{w} = (\hat{\mathbf{n}}_1 \cdot \mathbf{u}(\mathbf{x}_1), \hat{\mathbf{n}}_2 \cdot \mathbf{u}(\mathbf{x}_2))$ . For convenience we write  $U_i(\mathbf{r}) \equiv \langle u_i(\mathbf{x}_1) \delta(\mathbf{x}_2) \rangle$  and  $\Psi_{ij}(\mathbf{r}) = \langle u_i(\mathbf{x}_1) u_j(\mathbf{x}_2) \rangle$  for the velocity–density and velocity–velocity correlation functions. In terms of the (linear) power spectra,

$$U_i(\mathbf{s}) = \int \frac{d^3 \mathbf{k}}{(2\pi)^3} e^{-i\mathbf{k} \cdot \mathbf{s}} \frac{ik_i}{k^2} P_{\theta\delta}(k) = -\partial_i \int \frac{k^2 dk}{2\pi^2} \frac{1}{k^2} j_0(ks) P_{\theta\delta}(k), \quad (\text{C2})$$

$$\Psi_{ij}(\mathbf{s}) = \int \frac{d^3 \mathbf{k}}{(2\pi)^3} e^{-i\mathbf{k} \cdot \mathbf{s}} \frac{ik_i}{k^2} \frac{-ik_j}{k^2} P_{\theta\theta}(k) = -\partial_i \partial_j \int \frac{k^2 dk}{2\pi^2} \frac{1}{k^4} j_0(ks) P_{\theta\theta}(k), \quad (\text{C3})$$

where  $\theta$  is the velocity divergence,  $\partial_i = \partial/\partial s_i$ , and we have used that  $u_i = ik_i/k^2 \theta$  (for a potential flow). Recall that the separation  $\mathbf{r} = \mathbf{x}_1 - \mathbf{x}_2$  is given in terms of the radial distances as  $\mathbf{r}(\boldsymbol{\chi}') = \chi_1' \hat{\mathbf{n}}_1 - \chi_2' \hat{\mathbf{n}}_2$ , and in redshift space  $\mathbf{s}(\boldsymbol{\chi}) = \chi_1 \hat{\mathbf{n}}_1 - \chi_2 \hat{\mathbf{n}}_2 = \mathbf{r}(\boldsymbol{\chi})$ .

To evaluate Eq. (C1), we expand the generator and keep only up to quadratic terms:

$$\begin{aligned} & \langle (1 + b_A \delta_1)(1 + b_B \delta_2) e^{i\boldsymbol{\kappa} \cdot \mathbf{w}} \rangle \\ & \simeq 1 + \xi(r) + i\boldsymbol{\kappa}_a \langle w_a (b_A \delta_1 + b_B \delta_2) \rangle - \frac{1}{2} \boldsymbol{\kappa}_a \boldsymbol{\kappa}_b \langle w_a w_b \rangle \\ & = 1 + \xi(r) + i(b_B \kappa_1 \hat{n}_1^i - b_A \kappa_2 \hat{n}_2^i) U_i(\mathbf{r}) \\ & \quad - \kappa_1 \kappa_2 \hat{n}_1^i \hat{n}_2^j \Psi_{ij}(\mathbf{r}), \end{aligned} \quad (\text{C4})$$

where we have dropped zero-lag terms since they are absent in the linear predictions. Here we have used that  $\langle \mathbf{u}_2 \delta_1 \rangle = -\langle \mathbf{u}_1 \delta_2 \rangle$ , and  $\langle \mathbf{u}_1 \delta_1 \rangle = \langle \mathbf{u}_2 \delta_2 \rangle = 0$ , which follow from isotropy of the underlying fields.

We will now evaluate Eq. (C1) using the expansion (C4). This is a two-step calculation: first evaluate the  $\boldsymbol{\kappa}$  integral to yield a Dirac delta function, then evaluate the radial integrals. First, focus on the  $U_i$  term in Eq. (C4); applying the  $\kappa_i$  integral on this we have

$$\begin{aligned} & \int \frac{d^2 \boldsymbol{\kappa}}{(2\pi)^2} e^{-i\boldsymbol{\kappa} \cdot (\boldsymbol{x} - \boldsymbol{x}')} i(b_B \kappa_1 \hat{\mathbf{n}}_1 - b_A \kappa_2 \hat{\mathbf{n}}_2) \cdot \mathbf{U}(\mathbf{r}) \\ & = \mathbf{U}(\mathbf{r}) \cdot \left( b_A \hat{\mathbf{n}}_2 \frac{\partial}{\partial \chi_2} - b_B \hat{\mathbf{n}}_1 \frac{\partial}{\partial \chi_1} \right) \delta_D(\boldsymbol{\chi} - \boldsymbol{\chi}'). \end{aligned}$$

Inserting this back into the line-of-sight integrals and doing the integration with the help of the delta functions, we obtain

$$\begin{aligned} & \frac{1}{\chi_1^2 \chi_2^2} \left( b_A \frac{\partial}{\partial \chi_2} \hat{\mathbf{n}}_2 - b_B \frac{\partial}{\partial \chi_1} \hat{\mathbf{n}}_1 \right) \cdot \chi_1^2 \chi_2^2 \mathbf{U}(\mathbf{s}) \\ & = b_A \frac{1}{\chi_2^2} \frac{\partial}{\partial \chi_2} (\chi_2^2 \mathbf{U}) \cdot \hat{\mathbf{n}}_2 - b_B \frac{1}{\chi_1^2} \frac{\partial}{\partial \chi_1} (\chi_1^2 \mathbf{U}) \cdot \hat{\mathbf{n}}_1. \end{aligned}$$

Note that  $\partial s/\chi_1 = \hat{\mathbf{n}}_1 \cdot \nabla s = \hat{\mathbf{n}}_1 \cdot \hat{\mathbf{s}}$  and  $\partial s/\chi_2 = -\hat{\mathbf{n}}_2 \cdot \nabla s = -\hat{\mathbf{n}}_2 \cdot \hat{\mathbf{s}}$ . Next, the  $\Psi_{ij}$  term in Eq. (C4); plugging this into the  $\kappa_i$  integral gives

$$\begin{aligned} & -\frac{1}{2} \int \frac{d^2 \boldsymbol{\kappa}}{(2\pi)^2} e^{-i\boldsymbol{\kappa} \cdot (\boldsymbol{x} - \boldsymbol{x}')} \kappa_1 \kappa_2 \hat{n}_1^i \hat{n}_2^j \Psi_{ij}(\mathbf{r}) \\ & = \Psi_{ij}(\mathbf{r}) \hat{n}_1^i \hat{n}_2^j \frac{\partial}{\partial \chi_1} \frac{\partial}{\partial \chi_2} \delta_D(\boldsymbol{\chi} - \boldsymbol{\chi}'). \end{aligned}$$

Inserting this back into Eq. (C1) and doing the radial integrals we have

$$\begin{aligned} & \frac{1}{\chi_1^2} \frac{\partial}{\partial \chi_1} \chi_1^2 \frac{1}{\chi_2^2} \frac{\partial}{\partial \chi_2} \chi_2^2 \Psi_{ij}(\mathbf{s}) \hat{n}_1^i \hat{n}_2^j \\ & = \left( \frac{\partial}{\partial \chi_1} \frac{\partial}{\partial \chi_2} + \frac{2}{\chi_1} \frac{\partial}{\partial \chi_2} + \frac{2}{\chi_2} \frac{\partial}{\partial \chi_1} + \frac{2}{\chi_1 \chi_2} \right) \Psi_{ij}(\mathbf{s}) \hat{n}_1^i \hat{n}_2^j, \end{aligned}$$

where the second and third terms on the right-hand side are order  $\mathcal{H}/k$ , while the last is order  $(\mathcal{H}/k)^2$ .

Altogether we have

$$\begin{aligned} \xi_s(\chi_1, \chi_2, \hat{\mathbf{n}}_1 \cdot \hat{\mathbf{n}}_2) & = b_A b_B \xi(s) - b_B \frac{1}{\chi_1^2} \frac{\partial}{\partial \chi_1} \chi_1^2 U_i \hat{n}_1^i \\ & \quad + b_A \frac{1}{\chi_2^2} \frac{\partial}{\partial \chi_2} \chi_2^2 U_i \hat{n}_2^i \\ & \quad + \frac{1}{\chi_1^2} \frac{\partial}{\partial \chi_1} \chi_1^2 \frac{1}{\chi_2^2} \frac{\partial}{\partial \chi_2} \chi_2^2 \Psi_{ij} \hat{n}_1^i \hat{n}_2^j, \end{aligned} \quad (\text{C5})$$

where  $\xi$ ,  $U_i$ , and  $\Psi_{ij}$  depend on  $\chi_1$  and  $\chi_2$  through  $\mathbf{s}$ , and we remember that  $\partial \hat{n}^i / \partial \chi = 0$ , i.e. lines of sight are always constant with respect to their radial derivatives. This equation is the wide-angle formula for the linear correlation function and as we just saw the last derivative produces an order  $(\mathcal{H}/k)^2$  term that we will henceforth ignore. Evaluating the derivatives in Eq. (C5) yields Eq. (56) in the main text.

We now move onto computing the wide-angle corrections. For this it is convenient to switch to Cartesian coordinates, noting that for any function  $f(\mathbf{s})$ , with  $\mathbf{s} = \mathbf{s}_1 - \mathbf{s}_2$ , we have by the chain rule  $\partial f / \partial \chi_1 = \hat{n}_1^j \partial_j f$  and  $\partial f / \partial \chi_2 = -\hat{n}_2^j \partial_j f$ , since  $\partial s_1^j / \partial \chi_1 = \hat{n}_1^j$  and  $\partial s_2^j / \partial \chi_2 = \hat{n}_2^j$ . With these, Eq. (56) becomes

$$\begin{aligned}
\xi_s(\chi_1, \chi_2, \hat{\mathbf{n}}_1 \cdot \hat{\mathbf{n}}_2) &= b_A b_B \xi(s) - (b_B \hat{n}_1^i \hat{n}_1^j + b_A \hat{n}_2^i \hat{n}_2^j) \partial_i U_j \\
&\quad - \hat{n}_1^i \hat{n}_2^j \hat{n}_1^k \hat{n}_2^l \partial_k \partial_l \Psi_{ij} \\
&\quad - b_B \frac{2}{\chi_1} U_i \hat{n}_1^i + b_A \frac{2}{\chi_2} U_i \hat{n}_2^i \\
&\quad + \left( \frac{2}{\chi_1} \hat{n}_1^k - \frac{2}{\chi_2} \hat{n}_2^k \right) \partial_k \Psi_{ij} \hat{n}_1^i \hat{n}_2^j, \quad (\text{C6})
\end{aligned}$$

where as a shorthand  $\partial_i \equiv \partial/\partial s_i$ . Note that when  $b_A = b_B$  the wide-angle corrections enter terms in the first line at second order in  $\epsilon$ , and when  $b_A \neq b_B$  they enter at first order in  $\epsilon$ .

It now remains to compute the multipoles. We will first compute the zeroth-order multipoles, i.e. the usual Kaiser multipoles, then the first-order multipoles that are associated with the wide-angle contributions. The following derivatives will be needed:

$$\frac{1}{k^2} \partial_m \partial_n j_0(ks) = -\frac{j_1(ks)}{ks} \delta_{mn} + j_2(ks) \hat{s}_m \hat{s}_n, \quad (\text{C7a})$$

$$\begin{aligned}
\frac{1}{k^3} \partial_j \partial_m \partial_n j_0(ks) &= \frac{j_2(ks)}{ks} (\hat{s}_j \delta_{mn} + 2 \text{ perm.}) \\
&\quad - j_3(ks) \hat{s}_j \hat{s}_m \hat{s}_n, \quad (\text{C7b})
\end{aligned}$$

$$\begin{aligned}
\frac{1}{k^4} \partial_i \partial_j \partial_m \partial_n j_0(ks) &= \frac{j_2(ks)}{(ks)^2} (\delta_{ij} \delta_{mn} + 2 \text{ perm.}) \\
&\quad - \frac{j_3(ks)}{ks} (\hat{s}_i \hat{s}_j \delta_{mn} + 5 \text{ perm.}) \\
&\quad + j_4(ks) \hat{s}_i \hat{s}_j \hat{s}_m \hat{s}_n, \quad (\text{C7c})
\end{aligned}$$

where  $\partial_i \equiv \partial/\partial s_i$ . Note that  $(2\ell + 1)j_\ell(x)/x = j_{\ell-1}(x) + j_{\ell+1}(x)$ .

### 1. Distant-observer limit

To recover the Kaiser multipoles, set  $\hat{\mathbf{n}}_1 = \hat{\mathbf{n}}_2 = \mathbf{e}_z = (0, 0, 1)$ . Then Eq. (C6) simplifies to

$$\begin{aligned}
\xi_s(\chi_1, \chi_2, \hat{\mathbf{n}}_1 \cdot \hat{\mathbf{n}}_2) &= b_A b_B \xi(s) - (b_A + b_B) \partial_3 U_3 - \partial_3^2 \Psi_{33} \\
&\quad - \left( b_B \frac{2}{\chi_1} - b_A \frac{2}{\chi_2} \right) U_3 \\
&\quad + \left( \frac{2}{\chi_1} - \frac{2}{\chi_2} \right) \partial_3 \Psi_{33}. \quad (\text{C8})
\end{aligned}$$

In the distant-observer limit, we can immediately discard all terms order  $\epsilon$  and higher, namely, the last two terms in Eq. (C8), since with  $\chi \sim d$  and  $U \sim \partial\Psi \sim s$  they are  $\mathcal{O}(\epsilon)$ . The remaining terms evaluate to Eqs. (58a) and (58b) in the main text, and from these equations it is straightforward to assemble the Kaiser multipoles (52). Note that for the

autocorrelation function ( $b_A = b_B$ ), wide-angle effects enter the multipoles at  $\epsilon^2$ , not order  $\epsilon$ . This is only true in the midpoint (and bisector) parametrizations, however.

### 2. Wide-angle contributions at leading order

Referring back to Eq. (C6), wide-angle corrections enter the terms  $U$  and  $\partial U$  at order  $\epsilon$ . By contrast, wide-angle corrections enter the  $\partial\Psi$  and  $\partial^2\Psi$  terms at order  $\epsilon^2$ , so do not need to be considered further in this leading-order calculation.

The fact that the corrections are not all second order is a consequence of the bias parameters spoiling invariance of the correlations under pair interchange. We thus need only focus on the  $U_i$  terms. To develop Eq. (C6) further we use the leading-order expressions  $\hat{\mathbf{n}}_1 = \mathbf{e}_z + \frac{\epsilon}{2} \mathbf{n}^{(1)}$  and  $\hat{\mathbf{n}}_2 = \mathbf{e}_z - \frac{\epsilon}{2} \mathbf{n}^{(1)}$ , where  $\mathbf{n}^{(1)} = -\sqrt{1-\mu^2} \mathbf{e}_x$ . For the  $\partial_i U_j$  term in Eq. (C6) we have, with the help of Eq. (C7a),

$$\begin{aligned}
&(b_B \hat{n}_1^i \hat{n}_1^j + b_A \hat{n}_2^i \hat{n}_2^j) \partial_i U_j \\
&= (b_A + b_B) \int \frac{k^2 dk}{2\pi^2} \left( \frac{1}{3} j_0(ks) - \frac{2}{3} j_2(ks) \mathcal{L}_2(\mu) \right) P_{\theta\delta}(k) \\
&\quad + \frac{2}{5} \epsilon (b_B - b_A) \int \frac{k^2 dk}{2\pi^2} (-\mathcal{L}_1(\mu) + \mathcal{L}_3(\mu)) j_2(ks) P_{\theta\delta}(k), \quad (\text{C9})
\end{aligned}$$

where the second term in this expression is the wide-angle correction (which agrees with Eqs. (52) and (53) in Ref. [12]; see also Eq. (3.19) in Ref. [46]). For the  $U_i$  terms in Eq. (56) we use Eq. (C2) and contract with the appropriate line of sight. The result is Eq. (60). Gathering these results together, it is a straightforward exercise to construct the multipoles (61).

## APPENDIX D: END-POINT PARAMETRIZATION

The end-point parametrization is less symmetric than the midpoint parametrization (it induces odd multipoles) but is often preferred for practical reasons, e.g. for power-spectrum estimation [47,48]. For completeness, in this appendix we derive the relation between the multipoles in the midpoint parametrization (used in this work) and that in the endpoint parametrization, denoted  $\xi_\ell$  and  $\xi_\ell^{\text{ep}}$ , respectively.

In general, the (cosine of the) angular separation can be defined as  $\mu = \hat{\mathbf{d}} \cdot \hat{\mathbf{s}}$ . In the midpoint parametrization  $\hat{\mathbf{d}} = \mathbf{e}_z$ , while in the end-point parametrization  $\hat{\mathbf{d}} = \hat{\mathbf{n}}_1$  (or alternatively  $\hat{\mathbf{d}} = \hat{\mathbf{n}}_2$ ); see Fig. 3. Based on a trigonometric analysis of Fig. 1, we find that the separations are related by



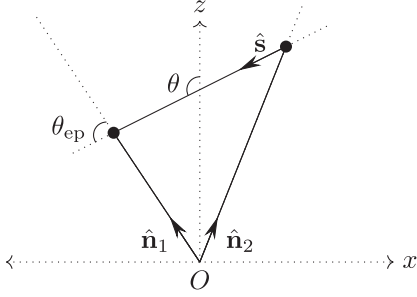


FIG. 3. Comparison of end-point separation  $\cos \theta_{\text{ep}} = \mu_{\text{ep}} = \hat{\mathbf{n}}_1 \cdot \hat{\mathbf{s}}$  and the midpoint separation  $\cos \theta = \mu = \mathbf{e}_z \cdot \hat{\mathbf{s}}$ .

$$\begin{aligned} \mu &= \mu_{\text{ep}} + \frac{\epsilon}{2}(\mu^2 - 1) + \mathcal{O}(\epsilon^2), \\ \mu_{\text{ep}} &= \mu - \frac{\epsilon}{2}(\mu^2 - 1) + \mathcal{O}(\epsilon^2). \end{aligned} \quad (\text{D1})$$

The expansion parameter in the end-point parametrization is  $\epsilon_{\text{ep}} \equiv s/s_1$  and  $\epsilon_{\text{ep}} = \epsilon + \mathcal{O}(\epsilon^2)$ ; since we will be working to leading order we may use  $\epsilon_{\text{ep}}$  or  $\epsilon$  interchangeably.

The relation between Legendre polynomials in the midpoint and end-point parametrizations is at leading order (for  $\ell \geq 1$ )

$$\begin{aligned} \mathcal{L}_\ell(\mu) &= \mathcal{L}_\ell\left(\mu_{\text{ep}} + \frac{1}{2}\epsilon(\mu_{\text{ep}}^2 - 1)\right) \\ &\simeq \mathcal{L}_\ell(\mu_{\text{ep}}) + \frac{\epsilon}{2}(\mu_{\text{ep}}^2 - 1) \frac{d\mathcal{L}_\ell}{d\mu_{\text{ep}}} \\ &= \mathcal{L}_\ell(\mu_{\text{ep}}) + \frac{\epsilon}{2}\ell(\mu_{\text{ep}}\mathcal{L}_\ell(\mu_{\text{ep}}) - \mathcal{L}_{\ell-1}(\mu_{\text{ep}})), \end{aligned}$$

where in the last equality we have used the recursion relation  $(x^2 - 1)d\mathcal{L}_\ell/dx = \ell(x\mathcal{L}_\ell(x) - \mathcal{L}_{\ell-1}(x))$ . Thus, at leading order in  $\epsilon$  we have

$$\begin{aligned} \xi_s(s, \mu) &\equiv \sum_\ell \xi_\ell^{(0)}(s) \mathcal{L}_\ell(\mu) \\ &= \sum_\ell \xi_\ell^{(0)}(s) \left[ \mathcal{L}_\ell(\mu_{\text{ep}}) \right. \\ &\quad \left. + \frac{\epsilon}{2}\ell(\mu_{\text{ep}}\mathcal{L}_\ell(\mu_{\text{ep}}) - \mathcal{L}_{\ell-1}(\mu_{\text{ep}})) \right]. \end{aligned}$$

Therefore, the multipoles in the midpoint parametrization are related to those in the end-point parametrization by

$$\begin{aligned} \xi_\ell^{\text{ep}}(s) &\equiv \frac{2\ell + 1}{2} \int_{-1}^1 d\mu_{\text{ep}} \mathcal{L}_\ell(\mu_{\text{ep}}) \xi_s(s, \mu) \\ &= \xi_\ell^{(0)}(s) + \epsilon \sum_{\ell'} M_{\ell\ell'} \xi_{\ell'}^{(0)}(s) + \mathcal{O}(\epsilon^2), \end{aligned} \quad (\text{D2})$$

where the coupling coefficients are given by

$$\begin{aligned} M_{\ell\ell'} &\equiv \frac{1}{2} \frac{2\ell + 1}{2} \int_{-1}^1 d\mu_{\text{ep}} \mathcal{L}_\ell(\mu_{\text{ep}}) \\ &\quad \times \ell'(\mu_{\text{ep}}\mathcal{L}_{\ell'}(\mu_{\text{ep}}) - \mathcal{L}_{\ell'-1}(\mu_{\text{ep}})). \end{aligned} \quad (\text{D3})$$

The nonzero coefficients are  $M_{12} = -3/5$ ,  $M_{32} = 3/5$ , and  $M_{34} = -10/9$ , i.e. the only induced multipoles (at order  $\epsilon$ ) are for  $\ell = 1, 3$ , the dipole and octupole:

$$\xi_1^{\text{ep}(1)} = -\frac{3}{5}\xi_2^{(0)}, \quad \xi_3^{\text{ep}(1)} = \frac{3}{5}\xi_2^{(0)} - \frac{10}{9}\xi_4^{(0)},$$

i.e. there is a leakage of the even multipoles into the odd multipoles. This expression agrees with Eq. (4.14) in Ref. [44] upon inserting the Kaiser multipoles (52).

- 
- [1] T. Baker, A. Barreira, H. Desmond, P. Ferreira, B. Jain *et al.*, Novel probes project: Tests of gravity on astrophysical scales, *Rev. Mod. Phys.* **93**, 015003 (2021).
- [2] N. Kaiser, Clustering in real space and in redshift space, *Mon. Not. R. Astron. Soc.* **227**, 1 (1987).
- [3] A. J. S. Hamilton, Measuring omega and the real correlation function from the redshift correlation function, *Astrophys. J. Lett.* **385**, L5 (1992).
- [4] A. Aghamousa, J. Aguilar, S. Ahlen, S. Alam, L. E. Allen *et al.* (DESI Collaboration), The DESI experiment part I: Science, targeting, and survey design, arXiv:1611.00036.
- [5] C. Hahn, M. J. Wilson, O. Ruiz-Macias, S. Cole, D. H. Weinberg *et al.*, The DESI bright galaxy survey: Final target selection, design, and validation, *Astron. J.* **165**, 253 (2023).
- [6] A. Raccanelli, L. Samushia, and W. J. Percival, Simulating redshift-space distortions for galaxy pairs with wide angular separation, *Mon. Not. R. Astron. Soc.* **409**, 1525 (2010).
- [7] J. Yoo, A. L. Fitzpatrick, and M. Zaldarriaga, A new perspective on galaxy clustering as a cosmological probe: General relativistic effects, *Phys. Rev. D* **80**, 083514 (2009).
- [8] C. Bonvin and R. Durrer, What galaxy surveys really measure, *Phys. Rev. D* **84**, 063505 (2011).
- [9] A. Challinor and A. Lewis, The linear power spectrum of observed source number counts, *Phys. Rev. D* **84**, 043516 (2011).
- [10] D. Jeong, F. Schmidt, and C. M. Hirata, Large-scale clustering of galaxies in general relativity, *Phys. Rev. D* **85**, 023504 (2012).

- [11] P. McDonald, Gravitational redshift and other redshift-space distortions of the imaginary part of the power spectrum, *J. Cosmol. Astropart. Phys.* **11** (2009) 026.
- [12] C. Bonvin, L. Hui, and E. Gaztanaga, Asymmetric galaxy correlation functions, *Phys. Rev. D* **89**, 083535 (2014).
- [13] C. Bonvin, Isolating relativistic effects in large-scale structure, *Classical Quantum Gravity* **31**, 234002 (2014).
- [14] E. Castorina and M. White, Beyond the plane-parallel approximation for redshift surveys, *Mon. Not. R. Astron. Soc.* **476**, 4403 (2018).
- [15] A. N. Taylor and A. J. S. Hamilton, Non-linear cosmological power spectra in real and redshift space, *Mon. Not. R. Astron. Soc.* **282**, 767 (1996).
- [16] T. Matsubara, Nonlinear perturbation theory with halo bias and redshift-space distortions via the Lagrangian picture, *Phys. Rev. D* **78**, 083519 (2008); **78**, 109901(E) (2008).
- [17] T. Baldauf, M. Mirbabayi, M. Simonović, and M. Zaldarriaga, Equivalence principle and the baryon acoustic peak, *Phys. Rev. D* **92**, 043514 (2015).
- [18] A. Taruya, S. Saga, M.-A. Breton, Y. Rasera, and T. Fujita, Wide-angle redshift-space distortions at quasi-linear scales: cross-correlation functions from Zel'dovich approximation, *Mon. Not. R. Astron. Soc.* **491**, 4162 (2019).
- [19] S. Saga, A. Taruya, M.-A. Breton, and Y. Rasera, Modelling the asymmetry of the halo cross-correlation function with relativistic effects at quasi-linear scales, *Mon. Not. R. Astron. Soc.* **498**, 981 (2020).
- [20] S. Saga, A. Taruya, Y. Rasera, and M.-A. Breton, Detectability of the gravitational redshift effect from the asymmetric galaxy clustering, *Mon. Not. R. Astron. Soc.* **511**, 2732 (2022).
- [21] V. Tansella, C. Bonvin, R. Durrer, B. Ghosh, and E. Sellentin, The full-sky relativistic correlation function and power spectrum of galaxy number counts. Part I: Theoretical aspects, *J. Cosmol. Astropart. Phys.* **03** (2018) 019.
- [22] C. Bonvin, F. Lepori, S. Schulz, I. Tutusaus, J. Adamek, and P. Fosalba, A case study for measuring the relativistic dipole of a galaxy cross-correlation with the dark energy spectroscopic instrument, *Mon. Not. R. Astron. Soc.* **525**, 4611 (2023).
- [23] F. Beutler and E. Di Dio, Modeling relativistic contributions to the halo power spectrum dipole, *J. Cosmol. Astropart. Phys.* **07** (2020) 048.
- [24] E. Di Dio and F. Beutler, The relativistic galaxy number counts in the weak field approximation, *J. Cosmol. Astropart. Phys.* **09** (2020) 058.
- [25] M. Noorikuhani and R. Scoccimarro, Wide-angle and relativistic effects in Fourier-space clustering statistics, *Phys. Rev. D* **107**, 083528 (2023).
- [26] R. Scoccimarro, Redshift-space distortions, pairwise velocities, and nonlinearities, *Phys. Rev. D* **70**, 083007 (2004).
- [27] P. J. E. Peebles, *The Large-Scale Structure of the Universe* (Princeton University Press, Princeton, NJ, 1980).
- [28] B. A. Reid and M. White, Towards an accurate model of the redshift-space clustering of haloes in the quasi-linear regime, *Mon. Not. R. Astron. Soc.* **417**, 1913 (2011).
- [29] J. Carlson, B. Reid, and M. White, Convolution Lagrangian perturbation theory for biased tracers, *Mon. Not. R. Astron. Soc.* **429**, 1674 (2012).
- [30] L. Wang, B. Reid, and M. White, An analytic model for redshift-space distortions, *Mon. Not. R. Astron. Soc.* **437**, 588 (2013).
- [31] V. Desjacques, D. Jeong, and F. Schmidt, Large-scale galaxy bias, *Phys. Rep.* **733**, 1 (2018).
- [32] A. Raccanelli and Z. Vlah, Power spectrum in the cave, arXiv:2305.16278.
- [33] A. Raccanelli and Z. Vlah, The observed power spectrum & frequency-angular power spectrum, *Phys. Rev. D* **108**, 043537 (2023).
- [34] Z. Gao, A. Raccanelli, and Z. Vlah, On the asymptotic connection between full- and flat-sky angular correlators, *Phys. Rev. D* **108**, 043503 (2023).
- [35] A. Raccanelli, L. Samushia, and W. J. Percival, Simulating redshift-space distortions for galaxy pairs with wide angular separation, *Mon. Not. R. Astron. Soc.* **409**, 1525 (2010).
- [36] C. Bonvin, R. Durrer, and M. A. Gasparini, Fluctuations of the luminosity distance, *Phys. Rev. D* **73**, 023523 (2006); **85**, 029901(E) (2012).
- [37] C. Bonvin, F. O. Franco, and P. Fleury, A null test of the equivalence principle using relativistic effects in galaxy surveys, *J. Cosmol. Astropart. Phys.* **08** (2020) 004.
- [38] N. Kaiser, Measuring gravitational redshifts in galaxy clusters, *Mon. Not. R. Astron. Soc.* **435**, 1278 (2013).
- [39] L. Samushia, B. A. Reid, M. White, W. J. Percival, A. J. Cuesta *et al.*, The clustering of galaxies in the SDSS-III Baryon Oscillation Spectroscopic Survey: Measuring growth rate and geometry with anisotropic clustering, *Mon. Not. R. Astron. Soc.* **439**, 3504 (2014).
- [40] S. Satpathy, S. Alam, S. Ho, M. White, N. A. Bahcall *et al.*, The clustering of galaxies in the completed SDSS-III Baryon Oscillation Spectroscopic Survey: On the measurement of growth rate using galaxy correlation functions, *Mon. Not. R. Astron. Soc.* **469**, 1369 (2017).
- [41] P. Zarrouk, E. Burtin, H. Gil-Marín, A. J. Ross, R. Tojeiro *et al.*, The clustering of the SDSS-IV extended baryon oscillation spectroscopic survey DR14 quasar sample: Measurement of the growth rate of structure from the anisotropic correlation function between redshift 0.8 and 2.2, *Mon. Not. R. Astron. Soc.* **477**, 1639 (2018).
- [42] J. E. Bautista, R. Paviot, M. V. Magaña, S. de la Torre, S. Fromenteau *et al.*, The completed SDSS-IV extended baryon oscillation spectroscopic survey: Measurement of the BAO and growth rate of structure of the luminous red galaxy sample from the anisotropic correlation function between redshifts 0.6 and 1, *Mon. Not. R. Astron. Soc.* **500**, 736 (2020).
- [43] C. Uhlemann, M. Kopp, and T. Haugg, Edgeworth streaming model for redshift space distortions, *Phys. Rev. D* **92** (2015).
- [44] P. Reimberg, F. Bernardeau, and C. Pitrou, Redshift-space distortions with wide angular separations, *J. Cosmol. Astropart. Phys.* **01** (2016) 048.

- [45] K. B. Fisher, On the validity of the streaming model for the redshift-space correlation function in the linear regime, *Astron. J.* **448**, 494 (1995).
- [46] C. Bonvin and P. Fleury, Testing the equivalence principle on cosmological scales, *J. Cosmol. Astropart. Phys.* **05** (2018) 061.
- [47] R. Scoccimarro, Fast estimators for redshift-space clustering, *Phys. Rev. D* **92**, 083532 (2015).
- [48] F. Beutler, E. Castorina, and P. Zhang, Interpreting measurements of the anisotropic galaxy power spectrum, *J. Cosmol. Astropart. Phys.* **03** (2019) 040.